DETERMINING THE AGES, SOURCES, AND CONNECTIONS BETWEEN GROUNDWATERS AND SURFACE WATERS IN THE UPPER AND MIDDLE BABOCOMARI WATERSHED

by

Jonathan H. Hasenstab

A Thesis Submitted to the Faculty of the

DEPARTMENT OF HYDROLOGY AND ATMOSPHERIC SCIENCES

In Partial Fulfillment of the Requirements

For the Degree of

MASTER OF SCIENCE
WITH A MAJOR IN HYDROLOGY

In the Graduate College

THE UNIVERSITY OF ARIZONA

2025

THE UNIVERSITY OF ARIZONA
GRADUATE COLLEGE

As members of the Master's Committee, we certify that we have read the thesis prepared by: Jonathan Hans Hasenstab
titled: Determining The Ages, Sources, And Connections Between Groundwaters And Surface Waters In The Upper And Middle Babocomari Watershed

and recommend that it be accepted as fulfilling the thesis requirement for the Master's Degree.

Jennifer Mcintosh — Date: Aug 17, 2025

Ty Ferre (Aug 19, 2025 11:52:30 PDT)
Ty Ferre — Date: Aug 19, 2025

Andrew Salywon (Aug 19, 2025 18:37:56 PDT)
Andrew Salywon — Date: Aug 19, 2025

Final approval and acceptance of this thesis is contingent upon the candidate's submission of the final copies of the thesis to the Graduate College.

I hereby certify that I have read this thesis prepared under my direction and recommend that it be accepted as fulfilling the Master's requirement.

Jennifer Mcintosh — Date: Aug 17, 2025
Thesis Committee Chair
Hydrology and Atmospheric Sciences

Signature: Jonathan Hasenstab (Aug 15, 2025 13:50:33 PDT)
Email: hasenstabj@arizona.edu

Acknowledgements

I would like to thank the Cooperative Endangered Species Conservation Fund Traditional Section 6 Grant Segment 28 through the Arizona Department of Agriculture to Andrew Salywon at the Desert Botanical Garden in Phoenix for providing the funding that sustained this study. Additional funding for sample analysis was also graciously provided by the Santa Cruz National Resource Conservation District, as well as a small grant from the Patagonia Regional Community Fund at the Arizona Community Foundation. I would also like to thank the residents of Elgin, the owners and managing members of the Babacomari Ranch, and the members of The Nature Conservancy for their hospitality and gracious support of this study in permitting myself and my sampling group to sample from the wells and surface waters on their properties, as well as their personal insights into the hydrology of the Babocomari Watershed. I also thank the writers at the Patagonia Regional Times for their publication of my original request to sample in the area which put me in contact with many well owners interested in this study.

I would like to thank my research advisors, Dr. Jennifer McIntosh (University of Arizona) and Dr. Andrew Salywon (Desert Botanical Garden in Phoenix) for their support and guidance throughout this study and for their help in the various sampling trips conducted in the Babocomari Watershed, as well as fellow University of Arizona students Tong Guo and Paola Miramontes for their assistance in collecting samples, and laboratory coordinator Tim Corley for his help in facilitating my lab work in the Harshbarger building.

Lastly, I would like to thank my parents, Raymond and Deonita, as well as my brother, Atreyu, for their unwavering support throughout my academic career at the University of Arizona.

Contents

Abstract

Groundwater and surface water are two intimately connected water storage regimes whose interactions impact the economic and ecological health of the regions they sustain. However, many growing communities in the southwestern United States with evolving land use lack comprehensive hydrologic studies characterizing their water resources. One such region is the Babocomari Watershed in southeastern Arizona, home to the winery communities of Elgin and Sonoita, as well as the Babocomari Cienega and River that are crucial habitats for many rare and endangered species of flora and fauna. Determining the age, sources, and chemistry of waters in this area could inform water and ecosystem management policies through knowledge of recharge seasonality and vulnerability to modern contamination. This research builds upon previous studies in the area through the collection and analysis of groundwater and surface water samples within the Babocomari Watershed, which were analyzed for solute chemistry, stable water isotopes, and age tracers. Elgin groundwater appears to come from local winter and summer precipitation that has experienced evaporation, while surface waters in the Cienega reflect evaporated summer precipitation. This seasonality can be affected by climate change, which shifts precipitation patterns and thus both the timing and magnitude of recharge. Principal Component Analysis indicates that Babocomari Cienega waters are more chemically similar to waters along O'Donnell Creek than waters from Elgin, implying the Cienega receives more water from the former than the latter. Groundwater in the upper and middle watershed is relatively young, with modern corrected radiocarbon signatures less than 500 years old. Some groundwaters also had detectable tritium, implying they contained a component of modern (post-1950s) recharge. Groundwater with modern recharge is susceptible to modern contamination, like nitrate from leaky septic tanks—a common problem in rural areas lacking centralized sewage infrastructure. Elevated nitrate levels were found in two wells in the Elgin area, with their nitrate isotope values consistent with septic contamination.

Introduction

Although groundwater and surface water are often treated as separate entities, the two are intimately connected regimes of water resources which can have direct impacts on one another through processes like recharge, discharge, contamination, and conservation. Nowhere is this more pertinent than in the freshwater wetlands of the American Southwest, where groundwater can breach the Earth's surface to form springs, ponds, rivers, and wetlands with saturated soils that provide crucial habitats for many rare and endangered species of flora and fauna. These wetlands, also known as cienegas, naturally filter water and mitigate floods, with their health often closely tied to the quality and quantity of groundwater in the area. It is for this reason that many cienegas throughout the American Southwest have shrunk or otherwise disappeared entirely over the last few decades as a result of—among other factors—groundwater overextraction, habitat modification, and climate change (Hendrickson & Minkley, 1985; Minkley et al., 2013).

Groundwater overextraction is a major concern for many communities in states like Arizona, where groundwater makes up 41% of the water supply (ADWR, 2020). Especially in communities facing increased groundwater drawdown, like Willcox, groundwater depletion from agricultural draws has caused land subsidence (ADWR, 2024) in addition to wells going dry as a result of lowered water tables (Myskow, 2023). Extrinsic factors like climate change are also projected to increase municipal and agriculture water demands due to higher temperatures and increased evapotranspiration (ADWR, 2023) while also shifting precipitation patterns (EPA, 2024a), with further research needed to determine how this could affect groundwater recharge (ADWR, 2023). Thus, proactive groundwater resource management will play a pivotal role in the ability of these communities to thrive in the coming decades.

The need for proactive groundwater management was made apparent last year in the Sonoita-Elgin area, located in Santa Cruz County of Southeastern Arizona. Starting in 2023, the Santa Cruz County Government announced a plan to promote tourism in the region through a "cuisine tourism initiative", which would use a $300,000 grant from the US Economic Development Administration to support the expansion of local restaurants, businesses, and the region's "fast-growing winery sector" (Santa Cruz County Government, 2024). However, the initiative faced extensive local backlash for numerous reasons, including concerns over how the plan's higher-density land zoning would affect the long-term sustainability of groundwater resources in the area (Davison, 2023; Vendituoli, 2024).

Groundwater resources in this region also affect the health of the Babocomari Cienega and River, located in the same watershed—the Babocomari Watershed—that encompasses much of the Sonoita-Elgin area, as well as the communities of Canelo, Sierra Vista, Fort Huachuca, and Huachuca City. The Babocomari Cienega is home to numerous important endangered species like the Canelo Hills ladies' tresses (*Spiranthes delitescens)*—an orchid that is an indicator of the cienega's health, which in turn is an indicator of the watershed's overall health. The presence of the Babocomari Cienega habitat hints at the crucial connections that exist between groundwaters and surface waters in this region—connections which have yet to be fully appreciated due to a lack of comprehensive groundwater and surface water studies in the Babocomari Watershed, and particularly within the Elgin-Sonoita communities.

Previous studies in Arizona have analyzed groundwater and surface water connections from a hydrogeochemical perspective, using stable water isotopes, age tracers, and water quality data to determine the location and seasonality of recharge, as well as the age and flow paths of groundwater feeding local wells and rivers. Therefore, by analyzing the quality, ages, sources, and connections of groundwaters and surface waters in the Babocomari Watershed, this study hopes to inform policies that can protect the Babocomari Watershed's water resources for years to come, and the communities, economies, and habitats they sustain. This study aims to provide a baseline water quality and chemistry dataset for regions of the watershed currently lacking such data, like within Elgin and along the Babocomari Cienega and River, with the aim of understanding the susceptibility of water resources in these areas to modern human influences like contamination or anthropogenic climate change.

Site Description

The Babocomari River Watershed is a 310-square-mile subwatershed of the Upper San Pedro River Basin located southeast of Tucson (Robinett & Kennedy, 2013). The general location of the Babocomari Watershed, in addition to the various sampling sites used for this study, are shown in *Figure 1a.*

Throughout its 25-mile course (Robinett & Kennedy, 2013), the Babocomari River is primarily ephemeral, meaning it only has flowing water immediately after precipitation events; however, some perennial reaches are fed by groundwater, like those supporting the river's cienega near the center of the watershed (Norman et al., 2019). The watershed's vegetation is dominated by Chihuahuan shrubs like creosote, in addition to semi-desert grasslands, localized forests, and woodlands (Robinett & Kennedy, 2013). Much of the watershed's vegetative variety can be found within the cienega itself, which supports willows, cottonwoods, shrubs, graminoids, and other interesting plants like Canelo Hills ladies' tresses orchids (Hendrickson & Minckley, 1985).

According to a 2001 geologic map of the Tucson and Nogales quadrangles by Peterson et al. (2001), much of the area surrounding the Babocomari River—from the upper watershed in the Elgin area to the lower watershed at its confluence with the San Pedro—is overlain by Quaternary and Neogene alluvium and sedimentary rocks, with the most downstream portion of the watershed in contact with Cretaceous volcanic andesites. The Mustang Mountains in the northern part of the watershed consist of Jurassic rhyolitic and andesitic volcanic rock, as well as Permian limestones, dolomites, sandstones, quartzites, and shales. The Canelo Hills to the southwest are of similar composition as the Mustang Mountains and exhibit extensive faulting and folding, with some Cretaceous sedimentary rocks. The Huachuca Mountains to the southeast also exhibit faulting and folding, with Proterozoic granites in contact with Cretaceous and Jurassic Bisbee Group rocks, as well as Miocene sedimentary rocks and Rillito Andesite.

The Babocomari Watershed encompasses numerous communities south of Arizona State Route 82, including Elgin, Canelo, Fort Huachuca, and Huachuca City, with some land owned by the Bureau of Land Management (USDOI: BLM 2022). The watershed also includes the 28,000-acre Babacomari Ranch, the "largest contiguous private land parcel in Arizona" (*Babacomari Ranch,* n.d.*)*. Groundwater samples for this study were primarily collected within the upstream community of Elgin—where land usage is dominated by private residential ranchettes and some agricultural plots that partially sustain the community's viticultural industry—as well as additional well and surface water samples collected along the Babocomari Cienega and River and a handful of surface water samples from O'Donnell Creek near Canelo. These data were combined with the datasets of Schwartzman (1990) in the lower Babocomari Watershed and Stratman (2022) in the O'Donnell Creek subwatershed to help contextualize all of these samples in the wider setting of the Babocomari Watershed at large.

Background on Major Environmental Tracers

The following section provides an overview of the different environmental tracers used in this and previous studies to analyze the hydrogeochemistry of the Babocomari Watershed.

Major Ion Chemistry

Ions primarily enter natural waters through dissolution of rocks and minerals, although some ions also come from atmospheric or human inputs. Major ion chemistry encompasses those ions which make up the bulk of the chemistry in most natural groundwaters and surface waters, including cations like sodium (Na^{+}), potassium (K^{+}), calcium (Ca^{2+}), and magnesium (Mg^{2+}), as well as anions like fluoride (F^{-}), chloride (Cl^{-}), bromide (Br^{-}), bicarbonate (HCO_3^{-}), sulfate (SO_4^{2-}), nitrite (NO_2^{-}), nitrate (NO_3^{-}), and phosphate (PO_4^{3-}).

In addition to helping to detect natural or anthropogenic contamination, major ion chemistry also helps to identify the flow paths of natural waters. For example, in Arizona, many rocks are calcitic, meaning they are mostly composed of the mineral calcium carbonate—$CaCO_3$. Waters which flow through and dissolve these rocks will subsequently be abundant in calcitic ions: Ca^{2+}, CO_3^{2-}, and HCO_3^{-}. Since the hydrogeochemistry of natural waters tends to reflect the minerology of the rocks the water flowed through, one can compare the geology of a region with the major ion chemistry of water samples to identify what flow paths the water may have taken to eventually end up at the sampling site. A robust way to perform this kind of analysis is Principal Component Analysis, or PCA, which will be described in more detail in the **Methods** section.

Stable Water Isotopes (SWI)

The relative abundance of oxygen and hydrogen isotopes in water are expressed as delta ratios (δ^2H or $\delta^{18}O$) which describes how the ratio of heavy-to-light isotopes in the water compares to an existing standard called VSMOW[1] (and often reported in units of ‰ or "per mille", short for parts-per-thousand, since these variances tend to be very small). These stable water isotope (SWI) ratios in water tend to change when the water undergoes natural processes like evaporation and condensation, with evaporation leading to an increase in SWI values and condensation leading to a decrease (Ingraham, 1998).

The Global Meteoric Water Line (GMWL) represents the isotopic variation of precipitation around the globe (Craig, 1961), while Local Meteoric Water Lines (LMWLs), with variable slopes and intercepts, can be generated for precipitation samples from a specific region to reflect local differences in precipitation SWI values (Ingraham, 1998; Jasechko 2019). The SWI values of local surface and ground waters can then be compared to these lines to identify not only whether local water resources are recharged by local precipitation, but also the time of year when this recharge tends to occur (i.e., summer vs winter), elevation, and extent of evaporation (Jasechko, 2019).

Isotopic Age Tracers (Tritium, Radiocarbon, $\delta^{13}C$-DIC).

Tritium (^3H) and radiocarbon (^{14}C) are two common radioactive tracers used for determining the ages of natural waters—or, more specifically, the time that has elapsed since the water was last in contact with the atmosphere. Both tracers form naturally in the atmosphere, in addition to being released by nuclear weapons testing during the 1950s and 1960s (Jasechko, 2019). Tritium (^3H) is a radioactive trace isotope of hydrogen typically expressed in "tritium units" (TU)

[1] The Vienna Standard Mean Ocean Water (VSMOW) defines the zero point of the stable water isotope scale that is used to describe the relative abundance of ^2H to ^1H and ^{18}O to ^{16}O in water.

based on the radioactivity of the tritium in a liter of water (Jasechko, 2019). In Tucson, seasonal tritium in precipitation over the last two decades typically averaged around 3-5TU, although it has also been as low as 1TU and as high 8TU (University of Arizona Environmental Isotope Laboratory, 2022). Tritium has a relatively short half-life of 12.3 years, so groundwaters recharged prior to the 1950s (i.e., >75 years old) will have tritium concentrations falling below the detection limit (Jasechko, 2019) which was around 0.6TU in this thesis. Accordingly, water samples with detectable tritium contain some recharge from after the 1950s (<75 years old).

Radiocarbon (^{14}C) is a radioactive trace isotope of carbon typically expressed in units of "percent Modern Carbon" (pMC), with global groundwater radiocarbon values ranging from 0 to roughly 120 pMC (Jasechko, 2019). Radiocarbon's longer half-life of 5,730 years allows it to date waters recharged up to 50,000 years ago (Jasechko, 2019), though due to uncertainty in radiocarbon measurements and age corrections, the effective lower limit of radiocarbon dating is ~500 years (Stratman, 2022). In this paper, groundwater age ranges will be described as follows: "modern" water is any water recharged less than 75 years ago (i.e., after the 1950s), meaning it has detectable tritium; "submodern" water is any water recharged between 75 and 500 years ago, meaning it has no detectable tritium and falls below radiocarbon's effective dating range; "old" water is any water recharged more than 500 years ago via radiocarbon dating, and—in accordance with Jasechko (2019)—"fossil" water is any water recharged more than 11,700 years ago.

Groundwater ages from radiocarbon measurements must be corrected to account for extra "dead" carbon that the groundwater picks up from dissolving carbonate minerals underground (Han and Plummer, 2013; Jasechko, 2019). This correction involves measuring the water's stable carbon isotope ratio, or $\delta^{13}C$ of DIC (Dissolved Inorganic Carbon) in units of ‰ VPDB[2].

[2]The Vienna Peedee Belemnite (VPDB) isotope reference defines the zero point of the carbon stable isotope scale that is used to describe the relative abundance of ^{13}C and ^{12}C.

Carbonate minerals tend to have a higher δ^{13}C-DIC value than atmospheric carbon, so δ^{13}C-DIC on its own can be used as a qualitative age tracer, as older waters that have dissolved more carbonate minerals will tend to have higher δ^{13}C-DIC values (Han and Plummer, 2013; Jasechko, 2019). The δ^{13}C-DIC value can then be combined with the radiocarbon measurement to obtain a corrected radiocarbon age through the use of a spreadsheet developed by Han and Plummer (2013). This process will be described in more detail in the **Methods** section of this paper.

Nitrate Isotopes

Nitrate (NO_3^-) is considered a primary contaminant by the EPA, which limits its concentration in public water supplies to 45 mg/L as NO_3^- (or 10 mg/L as N)[3] to prevent blue baby syndrome (EPA, 2024b). Nitrate naturally exists in soils, with background nitrate levels in groundwater usually less than 4.5 mg/L as NO_3^- (Dubrovsky et al., 2010), while concentrations exceeding this amount typically indicate human activity (Dubrovsky et al., 2010). Anthropogenic nitrate sources include fertilizer runoff, leaky septic tanks, and manure/sewage (EPA, 2024b).

Kendall (1998) and Gibrilla et al. (2020) demonstrated that different sources of nitrate have distinct nitrate isotope signatures, meaning the $\delta^{15}N_{AIR}$[4] and $\delta^{18}O_{VSMOW}$ values in nitrate tend to fall into distinct ranges depending on whether that nitrate came from fertilizers, septic/manure, or natural soil nitrogen. This means that waters with elevated nitrate concentrations can be tested to determine the nitrate's source based on their nitrate isotope signatures.

[3]Nitrate levels are sometimes expressed in terms of the concentration of their nitrogen component ("mg/L as N"), rather than as the mass of the entire nitrate anion ("mg/L as NO_3^-"). For this paper, all remaining nitrate concentrations will be expressed as NO_3^-.
[4]AIR refers to atmospheric nitrogen (N_2), which is used as the zero point reference for the nitrogen isotope scale that describes the relative abundance of ^{15}N and ^{14}N.

Literature Review

The Babocomari Cienega is one of many important wetland habitats in the American Southwest threatened by declines in groundwater availability. Hendrickson & Minkley (1985) provides a backbone for research in this area through detailing the history of cienegas in the region and the benefits they provide to humans and the environment at large through acting as critical habitats for endangered species in otherwise arid environments, in addition to providing flood mitigation and natural water filtration. They describe the ongoing degradation of cienegas due to anthropogenic activity, with the number and extent of cienegas dwindling due to damming, ranching, livestock raising, urban development, and climate change. Minkley et al. (2013) goes into more detail on this point by showing that, of the 60 cienegas identified in their study area between southeastern Arizona, southwestern New Mexico, and northeastern Mexico, only 46 still had functioning ecosystems (i.e., not dried up and without significant disruption from their natural state), and of these 46, only nine had significant land management plans to ensure their protection. Both papers also note that groundwater decline—especially in regions of high irrigation and agricultural pumping—are a particular threat to cienegas, including the Babocomari Cienega.

To protect water resources in vulnerable areas like these, it is important to first characterize the age, sources, and quality of groundwaters and surface waters feeding these regions. Stable water isotopes, age tracers, and other hydrogeochemical constituents have previously been employed in southeastern Arizona for this purpose, with some studies encompassing areas adjacent to or within the Babocomari Watershed.

The Cienega Creek Watershed, north of the Babocomari Watershed, was the focus of a groundwater characterization study by Tucci (2018) to determine connections between groundwater in the area and recharge from the Santa Rita mountain system to the west. Using stable water isotope data, Tucci concluded that local precipitation had highly variable isotope compositions—possibly caused by variances in the precipitation's moisture source—and that the basin-fill aquifer that feeds Cienega Creek and adjacent wetlands itself was mainly fed by mountain-block recharge (defined as "percolation through the mountain bedrock that reaches the basin via the movement of deep groundwater", Wahi (2005)) from a mix of both winter and summer precipitation. The groundwater was mostly old to fossil age (i.e., tritium levels below the detection limit, corrected radiocarbon ages being a few hundred years old to over 15,000 years old), though a few samples showed mixing with modern water (i.e., water with some detectable tritium, implying a small component of recharge after the 1950s). Tucci concluded that the prevalence of old groundwater in the area and limited modern recharge could make the area's cienega and wildlife vulnerable to groundwater overextraction.

One of the studies cited in Tucci's report is Eastoe & Towne (2018), which outlined four groundwater recharge mechanisms throughout Arizona that create distinct patterns on stable water isotope plots, and how these patterns apply to major watersheds in the area. They characterized the Upper San Pedro (USP) basin as exhibiting two recharge patterns: Pattern 2 (where groundwater data plots slightly below the local meteoric water line (LMWL) since most infiltration occurs during the wettest 30% of both summer and winter months, when evaporation effects are muted and there is a decrease in the $\delta^{18}O$ and $\delta^{2}H$ values of precipitation); and Pattern 3 (where groundwater data follows the evaporation trend of whichever major river is located nearby). Their study included a plot showing how the average water isotope values of seasonal precipitation in Tucson vary with rainfall intensity, allowing for the construction of approximate LMWLs for study areas in southeastern Arizona lacking long-term precipitation data, like the Babocomari Watershed.

The researchers also provided an equation for the evaporation trend of the Upper San Pedro River, which can act as a basis of comparison for groundwater data in the Upper San Pedro Watershed.

The Babocomari Watershed is located within the Upper San Pedro Watershed, with the northern edge of the Babocomari Watershed abutting the boundary between the Upper and Middle San Pedro Watersheds. Geochemical and isotopic groundwater characterization was previously performed in both the Upper and Middle San Pedro River Watersheds by Wahi (2005) and Hopkins et al. (2014), respectively. To preface, Wahi (2005) notes that precipitation over mountains can recharge aquifers via two main mechanisms: the previously defined mountain-block recharge; and mountain-front recharge ("mountain runoff that infiltrates at the mountain front"); both together make up mountain-system recharge. Both Wahi (2005) and Hopkins et al. (2014) confirmed their respective subwatersheds had some mountain-system recharge that was a few years to a few decades old and primarily came from winter precipitation. Of particular note in the Hopkins et al. (2014) study is the prevalence of Ca-HCO_3 and Ca-Mg-HCO_3 waters in mountain-block samples, versus Ca-Na-HCO_3 to Na-HCO_3 type waters in lower basin fill aquifers, with the latter exhibiting mixing of summer and winter recharge via stable water isotope data, and corrected radiocarbon ages ranging from 1700 to 3700 years old. Wahi (2005) also noted significant evapotranspiration trends in the Upper San Pedro watershed as revealed by higher chloride concentrations in groundwater compared to precipitation. A previous paper in the same study area, Baillie (2005), reported that groundwater samples had small deviations of $\delta^{18}O$ from the LMWL, so Wahi (2005) argued that this, in tandem with the high chloride concentrations, meant transpiration dominated in the basin. Baillie (2005) conducted geochemical groundwater analysis in the Upper San Pedro and also found that basin groundwater primarily came from mountain-system winter recharge. Since this latter paper mainly analyzed groundwater contributions to the Upper San Pedro River's baseflow, its analyses could prove useful for future research on connections between groundwater in the Babocomari Watershed and surface waters within the Babocomari Cienega.

With regard to such research within Babocomari Watershed itself, most studies tended to focus on characterizing the watershed from a physical hydrology point of view, rather than from a hydrogeochemical perspective. Robinett & Kennedy (2013) detailed the Babocomari River Riparian Protection Project, a study funded by the Arizona Department of Water Resources (ADWR) which lasted from 2009 to 2013 and aimed to install fences to prevent livestock from accessing the river, and analyzed the cienega's temporal vegetation change, which they found to be minimal over the project's timeframe. In addition, the US Department of the Interior's Bureau of Land Management (USDOI: BLM) published an evaluation of the Babocomari area in 2022 with a focus on analyzing the Babocomari Cienega's quality. The BLM gave the cienega a Proper Functioning Condition (PFC) rating in 2018 based on its vegetation density and erosion resistance during high flow events; this was an improvement from 2013 when its lower reach was given a Functional-At-Risk (FAR) rating due to cattle grazing, which had contributed to bank and vegetation degradation—an issue later alleviated by improved livestock management.

Norman et al. (2019) focused on surface-water and groundwater interactions in the Babocomari Watershed through the installation of erosion-control structures (ECS), with the hopes of improving groundwater recharge and infiltration through erosion reduction. Though they found the resultant rise in recharge has the ability to increase baseflow in some reaches of the Babocomari River, the researchers acknowledged that most of the study focuses on shallow hydrologic processes, with conclusions on deep-aquifer recharge being drawn from model simulations. More recently, Montgomery & Associates and Natural Channel Design Engineering Inc. prepared a consultant's report to The Nature Conservancy titled *Babocomari Watershed Assessment* (2025), which detailed their assessment of physical hydrologic conditions in the Babocomari Watershed, with the aim of identifying areas in need of protection or restoration due to their vulnerability to problems like groundwater overextraction or channel degradation. The report drew upon models, satellite mapping and imagery, and in-situ visits to evaluate groundwater levels, precipitation and recharge distributions, and stream channel and ecological conditions throughout the watershed.

Information gleaned from these reports could be bolstered by additional hydrogeochemical and isotopic analysis of water resources in the Babocomari Watershed, which would help identify the ages, recharge seasonality, and vulnerability of water resources in the area to modern anthropogenic activities. Though some studies have done such analyses in the Babocomari Watershed before, they have often been relegated only to specific subregions of the watershed, rather than looking at the watershed as a whole. Schwartzman (1990) characterized groundwater in the lower Babocomari Watershed near Huachuca City, Fort Huachuca, and Sierra Vista. His study was motivated by a lack of data on the effects of groundwater extraction on the Babocomari River, despite its proximity to the more heavily documented San Pedro River. Thus, his thesis sought to characterize the effects of drawdown on the Babocomari River through estimating transmissivities and specific capacities for the basin-fill aquifer that acts as a source for most groundwater withdrawal in the region, as well as measuring ion concentrations in groundwater samples to determine flow paths and rates of well water level decline. However, his study did not use any tritium nor radiocarbon dating, which leaves out a crucial element for determining groundwater residence times in the area. Because his study only focused on the lower part of the watershed, Schwartzman also notes in the paper that additional research should be conducted in the upper watershed to paint a more comprehensive picture of the entire watershed’s health and groundwater/surface water interactions.

Stratman (2022) addressed part of this knowledge gap by characterizing groundwater in the O'Donnell Creek subwatershed, located in the southern part of the upper Babocomari Watershed and encompassing the community of Canelo. Mountain-front recharge dominates this area and exhibits a mix of summer and winter precipitation sources and an evaporation trend consistent with other southern Arizona study areas. Most groundwater samples were submodern to old, with some having ages ranging from 300 to 5,700 years as determined by corrected radiocarbon data; a few samples showed mixing of modern and submodern groundwaters. A transpiration trend of increasing chloride concentration with little change in $\delta^{18}O$ was also noted in the shallow piezometer samples of his O'Donnell Creek data, which agrees with the transpiration signals that Wahi (2005) identified in the Upper San Pedro Watershed. Nitrate concentrations were measured in Stratman's study but not included in his paper, though he shared the unpublished nitrate data via email (personal communication, February 16, 2024) to act as a basis of comparison for nitrate measurements in other parts of the Babocomari Watershed.

While Stratman's 2022 study rounds out groundwater characterization in the southern part of the upper Babocomari Watershed, there is still a notable lack of data in the northern part of the watershed where the growing community of Elgin is located, which is of particular interest given the expected growth in the area. Vukomanovic et al. (2019) projected Elgin's open landscapes and rolling hills would encourage more exurbanization in the future (i.e., increased land use change and development in response to people moving from urban to rural communities for their better viewscapes, in addition to a sense of privacy that accompanies larger distances between neighbors). Elgin's agricultural potential also plays a strong factor in the area's growth through its renowned winery industry, which—as detailed in the introduction—influenced the Santa Cruz County Government's "cuisine tourism initiative" (Santa Cruz County Government, 2024).

Previous groundwater studies have noted the lack of groundwater characterization in the Elgin area despite its projected growth. Naeser & St. John (1998) aimed to calculate a safe yield value[5] for groundwater consumption in the nearby Sonoita Valley out of concern that the region might face problems (e.g. water table declines, an increase in pumping costs, and environmental problems like land subsidence), similar to those in other developing communities experiencing groundwater overextraction. Though they divided the valley into two study areas—one focused on Sonoita and the other on Elgin and the upper portion of the Babocomari Watershed—they found that a lack of available hydrologic studies made it impossible to calculate a safe yield value for the Elgin region. Conversely, the projected water use needed to sustain contemporary residential zoning in the Sonoita area was found to be three times higher than what the area's groundwater surplus could provide, leading the researchers to recommend that measures should be taken to ensure long-term groundwater sustainability in the area. Another study, Knight (1996), factored in the water draw of Elgin and Sonoita to develop a water budget for the upper Cienega Creek Basin to the north. At the time, both communities were considered small enough that any increase in pumping would have mostly local effects like wells going dry, and little impact on the upper Cienega Creek as a whole, since that area received little recharge from the Sonoita/Elgin region. Although this was positive information for the Cienega Creek's groundwater sustainability, it gives no information with regard to Elgin's groundwater influence within the Babocomari Watershed, from which the community draws most of its water resources.

In the face of this data scarcity, collecting groundwater samples in the upper Babocomari Watershed from localities like Elgin, as well as along the Babocomari Cienega itself, will be an

[5] Safe yield is a sustainability goal in Arizona and elsewhere, where the amount of groundwater withdrawn ((i.e. from pumping) is equal to or less than the amount that is recharged to an aquifer. This goal helps avoid an unacceptable decline in the hydraulic head or deterioration in water quality in the aquifer.

invaluable addition when combined with datasets from other parts of the watershed, like from Stratman (2022) and Schwartzman (1990), to provide a more encompassing view of groundwater in the Babocomari Watershed as a whole.

Methods

Sampling Sites

Between 2023 and 2024, a total of 39 water samples were collected for this study across the upper Babocomari Watershed (including within Elgin), the middle Babocomari Watershed (along the Babocomari Cienega and River), and the O'Donnell Creek subwatershed. These samples include groundwater, surface water, shallow ground water (piezometer), and spring water samples. Each sample was given an ID indicating its sampling location (U = Upper Babocomari Watershed, M = Middle Babocomari Watershed, and O = O'Donnell Creek subwatershed) and sample type (G = Groundwater, S = Surface water, P = Piezometer, R = Spring). Some sampling sites were sampled multiple times on different dates, as indicated by an "a", "b", or "c" after their sample ID. As an example of the sample ID notation, a sample named "UG1b" would be a groundwater sample from the upper Babocomari Watershed, with the "b" indicating this is the second time the site was sampled from. The IDs, collection dates, times, and geographic coordinates of all samples collected for this study are shown in *Table 1*, as well as being labeled on a map in *Figure 1b.* GPS coordinates and elevations were collected using a Garmin eTrex® 10 handheld GPS[6].

All groundwater wells were first "purged" to ensure the water sampled from the well was fresh groundwater, as opposed to water that may have been sitting static in the well bore, which could alter its chemistry and radiocarbon content. Additionally, well samples were collected before the water had passed through any water softeners, as softeners alter the natural ionic composition of the groundwater drawn from the wells. Some wells also included storage and/or pressurization tanks through which the water passed before exiting a spigot, so more water had to be purged from

---

[6] Brand names are included for informational purposes and do not constitute an endorsement by the author or the University of Arizona.

these wells to ensure fresh groundwater was being sampled, rather than water that had been sitting in the tanks. Well water was typically sampled from an outside spigot closest to the well when possible, with the exception of samples UG10a/b, MG1, and MG3, where the wells were connected to solar panels or windmills which actively drew from the wells throughout the day and fed the well water through pipes into a nearby lake or storage tank from which cattle could drink; in these cases, the flow rate out of the well was not fast enough to do the purging process in a reasonable amount of time, though it was assumed that said process was not needed for these wells since they were already being drawn from throughout the day and thus would not have water sitting static in the wells or pipes for extended periods. For all of the aforementioned wells, any water samples that did not need to be filtered were collected immediately upon exiting the well spigots or pipes to ensure the water spent as little time as possible exposed to the open air, so as to avoid equilibration with the atmosphere which could affect measurements; for samples requiring filtration, the well water was first collected in a plastic bucket that was rinsed with the sample water beforehand so that the water could be field-filtered with syringes and put into sample bottles.

Shallow subsurface water was sampled using piezometers—long, thin tubes driven vertically into the ground with perforations on the end that allowed shallow subsurface water to flow through the tube. For samples that did not require filtration, water was pumped directly out of these piezometers and into the sampling bottles, while samples requiring filtration were first pumped into a plastic bucket that had been rinsed beforehand with the sample water before being syringe-filtered into the sampling bottles.

All surface and spring water samples were collected directly from the water bodies without need for pumping or a collection bucket, and syringe-filtered when necessary. MS3, MS4a/b, MS7a/b, CS1a/b, CS2, and CR1a/b/c were collected at sites with actively flowing water; MS2 and

MS6 were collected from smaller, standing bodies of water; and MS1 and MS5 were collected from marshy areas with soil water close to the surface, wherein small holes were dug about four inches deep and six inches wide, with samples collected from the water pooling into the holes.

Well Sampling Procedures

At each well, field water parameters (i.e., temperature in degrees Celsius, pH, electroconductivity "EC", and dissolved oxygen percentage "DO") were measured with handheld meters, and seven sample bottles were filled with well water for analysis of anions, cations, alkalinity, stable water isotopes ("SWI", or $\delta^{18}O$ and $\delta^{2}H$ of H_2O), $\delta^{13}C$-DIC, tritium (^{3}H), and radiocarbon (^{14}C).

To determine when the wells had been sufficiently purged, water was pumped into and allowed to continuously overflow from the rinsed sampling bucket, with probes from three handheld meters immersed in the bucket water and monitored until their readings stabilized. The meters used were an Oakton® pH 150 portable meter[7]; an Oakton® CON 150 portable meter[7]; and a YSI 550A Dissolved Oxygen Instrument[7]. Both Oakton® meters were calibrated one day prior to each sampling date, while the dissolved oxygen (DO) meter was recalibrated at each site to account for differing elevations, which could affect the DO readings. Once the readings on the meters stabilized, it was presumed that the well was sufficiently purged and was now drawing fresh groundwater, so the meters' readings were recorded.

After removing the meter probes from the bucket and rinsing them with deionized water to avoid cross contamination, a 60mL plastic syringe with a 0.45μm filter was then used to fill five small sample aliquots with water from the bucket. A new syringe and filter were used at each site;

---

[7] Brand names are included for informational purposes and do not constitute an endorsement by the author or the University of Arizona.

each syringe was rinsed three times with the well water before sample collection began. The five small sample aliquots included: a 30mL HDPE aliquot for alkalinity; a 30mL HDPE aliquot for anions; a 30mL nitric-acid-washed HDPE aliquot for cations, which was then acidified with two drops of optima-grade nitric acid to prevent cation precipitation; a 30mL glass aliquot for stable water isotopes (SWI); and a 30mL crimp-top glass aliquot for δ^{13}C-DIC. All aliquots were filled to the top with water to minimize the amount of air ("headspace") in each bottle. Afterwards, two more large sample bottles were each rinsed three times with well water before being filled with water straight from the well spigots/pipes with minimal headspace. The bottles included a 1L HDPE bottle for tritium and a 1L combusted amber glass bottle for radiocarbon. All water samples were placed inside ice-filled coolers until they could be brought back to a lab at the University of Arizona for storage in a refrigerator.

Sampling sites with elevated nitrate concentrations were revisited at a later date and re-sampled for nitrate isotopes to determine their nitrate source. In these cases, the wells were purged again, with the nitrate isotope samples collected from fresh well water in the rinsed collection bucket, syringe-filtered through a 0.2μm filter into a 30mL HDPE aliquot with minimal headspace, and stored on dry ice in a cooler to keep them frozen until they could be brought back to a lab at the University of Arizona for storage in a freezer. Major ion chemistry and SWI were also resampled at these wells to reaffirm that the nitrate concentration was still elevated at the time of resampling and that the water source of the wells had not changed.

Sample Analyses

Each of the bottles were sent to different labs for analysis. The alkalinity samples were analyzed by the author using a Mettler Toledo DL53 Titrator[8] within one to two days of collecting the samples. The anion and cation samples were delivered by hand to the Arizona Laboratory for Emerging Contaminants (ALEC) at the University of Arizona and analyzed using ion chromatography and an Inductively Coupled Plasma Mass Spectrometer (ICP-MS), respectively. The tritium, $\delta^{13}C$, and SWI samples were delivered by hand to the Environmental Isotope Laboratory (EIL) at the University of Arizona for analysis. The radiocarbon samples were shipped overnight on ice via FedEx[8] to the National Ocean Sciences Accelerator Mass Spectrometry Facility (NOSAMS) in Massachusetts for analysis; each of the radiocarbon bottles had their lids wrapped with parafilm to inhibit degassing of CO_2 and fluid leakage, and were placed inside a large cooler alongside smaller 500mL HDPE bottles that had been filled with frozen water to act as ice packs. (Although each of the glass radiocarbon bottles were wrapped in three layers of bubble wrap and extra padding was added to the shipment package for protection, four of the samples—*UG6a*, *UG10a, MG1,* and *MG2a*—broke during transit to the radiocarbon lab and could not be analyzed. While these sites were later revisited to recollect their radiocarbon samples, funding constraints limited the author's ability to analyze all of the collected samples, so it was later determined based on the results of previous radiocarbon analyses that the recollected radiocarbon samples would likely not need to be analyzed. This will be detailed later in the **Results** section). Lastly, the nitrate isotope samples were shipped overnight on dry ice via FedEx[8] to the

---

[8]Brand names are included for informational purposes and do not constitute an endorsement by the author or the University of Arizona.

Stable Isotope Facility (SIF) at the University of California, Davis for analysis by bacterial denitrification assay.

Additional information on the sampled wells—like their installation logs, the soil media through which the wells were drilled, and their well water depths—were collected from publicly-available information on the Arizona Wells 55[9] site.

Principal Component Analysis

Principal Component Analysis, or PCA, is a widely used statistical method which can "...reduce the dimensionality of a dataset consisting of a large number of interrelated variables, while retaining as much as possible of the variation present in the dataset" (Jolliffe, 2022, p. 1). In essence, it takes a large dataset with many variables and condenses it to focus on only those variables which contribute the most variation to the data, which helps with both graphing and identifying trends in the dataset. PCA can be used in any field where a researcher aims to simplify the analysis of a large dataset, with Kirk (2020) and Tritz (2021) from the Cienega Creek Watershed being two examples of PCA being used in previous hydrology theses to identify different water sources contributing to a wetland. PCA was used in this paper to help determine whether the Babocomari Cienega receives more of its headwaters from the upper Babocomari Watershed (near Elgin), or from the O'Donnell Creek subwatershed (near Canelo), with the general idea being that the chemistry of headwaters feeding the Cienega should be similar to the chemistry of waters within the Cienega itself.

The variables/tracers used in the PCA were the ion concentrations (e.g., bicarbonate alkalinity, calcium, sodium, etc.) measured in each sample. In concept, these concentrations should

[9]https://azwatermaps.azwater.gov/wellreg

vary based on where the sample was collected, and while a researcher might normally visualize this spatial variability for one ion at a time, it would be more helpful to visualize the variability across all ions and all samples simultaneously. This would normally be difficult to do in a single graph, since not only were the samples collected across three sampling locations (upper Babocomari Watershed, middle Babocomari Watershed, O'Donnell Creek subwatershed), but each sample was also analyzed for almost a dozen different ions. However, through using a machine-learning algorithm, PCA can identify which tracers contribute the most variation to the samples in the dataset and groups them together so that they can be plotted on a single, 2D graph. For example, the y-axis on a PCA graph could represent whichever combined tracers (called Principal Component 1, or PC1) contributed the most variability to the dataset; the x-axis would then be whichever combined tracers (called Principal Component 2, or PC2) contributed the second most variability to the dataset. Tracers contributing minimal variability can then be discarded from the analysis, as long as the resultant individual variability of the plotted PCs does not fall below "1/p" of the dataset's total variability, with "p" being the number of tracers used in the analysis (Tritz, 2021). All of the samples can then be plotted on this graph and color-coded based on sampling location to help visually identify where the variability in tracers coincided with variability in sampling location, with chemically similar waters plotting close to one another and chemically distinct waters plotting away from one another. Visually examining this graph would then reveal whether samples collected along the Babocomari Cienega plot close to (and are thus chemically similar to) waters in the Elgin area versus waters in the O'Donnell Creek subwatershed. For this study, the PCA analysis was executed using a module built-in to Python's machine learning library, Scikit-Learn.

Radiocarbon Correction

As described in the **Background** section, radiocarbon samples must be corrected for dead carbon using δ^{13}C-DIC in order to obtain a more accurate estimate of their radiocarbon age. Radiocarbon correction was performed using a spreadsheet developed by Han and Plummer (2013), which builds upon a radiocarbon correction model originally proposed by Fontes and Garnier (1979). The corrected radiocarbon age of a given sample was obtained by taking its δ^{13}C-DIC and radiocarbon measurements—as well as its bicarbonate, carbonic acid (H_2CO_3), and carbonate (CO_3^{2-}) concentrations—and inputting them into the spreadsheet, whereupon it calculates the corrected age of the samples in years.

Because samples for this study did not have their carbonic acid and carbonate concentrations measured directly, these values were instead calculated using PHREEQC[10], a geochemical modeling program made by the USGS which can take inputs for a sample's major ion chemistry (alkalinity, cations, anions) and estimate the concentrations of other ions in the sample based on various built-in geochemical reaction simulations.

Additionally, the radiocarbon correction spreadsheet also requires inputs for the expected radiocarbon and δ^{13}C-DIC concentrations of both carbonate minerals and soil gas in the sampling area, as well as their associated uncertainty values. Based on similar radiocarbon analyses done by Stratman (2022) along O'Donnell Creek, the following values were assumed to apply for the radiocarbon correction: for carbonate minerals, δ^{13}C-DIC = -1‰ and ^{14}C = 0 pMC; for soil gas, δ^{13}C = -23‰ and ^{14}C = 100 pMC; and for uncertainty, δ^{13}C-DIC = 2‰ and ^{14}C = 5 pMC.

[10]https://www.usgs.gov/software/phreeqc-version-3

Results and Discussion

Regional Water Table Elevation and Water Table Depths

A kriged water table elevation map *(Figure 2)* was created by subtracting Wells 55 depth-to-water measurements from each sampling site's elevation using data from this study, as well as data from Schwartzman (1990), and Stratman (2022). The model's contours indicate groundwater generally flows northeastward towards the San Pedro River, with the upper Babocomari River initially flowing perpendicular to groundwater flow before becoming parallel to groundwater flow after its confluence with O'Donnell Creek. The gradients change in both direction and magnitude through the study area, with the upper watershed having steeper (0.01 to 0.02 ft/ft), more northerly gradients that become shallower (less than 0.005 ft/ft) and more easterly upon passing to the lower watershed. Note that the accuracy of this map is affected by the availability of sampling locations, with a lack of samples in the northern Babocomari Watershed near the Mustang Mountains and in the southern Babocomari Watershed near the Huachuca Mountains likely affecting the accuracy of the gradients (i.e., directions and magnitudes of groundwater flow) on this map. Montgomery & Associates and Natural Channel Design Engineering Inc. (2025) were able to capture the water table more accurately in these areas in their own water table map, which shows that beneath the Mustang Mountains and Huachuca Mountains, the water table exhibits mounding which would drive groundwater flow towards the Babocomari Cienega at the middle of the watershed—something not captured in *Figure 2.* However, both maps still show (1) general northeastern groundwater flow towards the San Pedro River, (2) groundwater gradients getting shallower near the lower Babocomari Watershed, and (3) groundwater flow being perpendicular to the upper Babocomari River, before becoming parallel past its confluence with O'Donnell Creek.

A separate point-water-table-depth map *(Figure 3)* was created by compiling data from Wells 55, which included many additional wells not sampled in this study, nor by Schwartzman (1990), nor Stratman (2022). The spatial accuracy of this map is again affected by the availability of data, with no point depth measurements within the Mustang Mountains and Huachuca Mountains. There seems to be a lot of spatial variation in point depths, although the map illustrates the expected trend of shallower water table depths along rivers. Drilling dates were not taken into consideration when creating this map, so it is possible that temporal changes in water table depth could cause the reported depth variations; however, some wells drilled within five years of one another were found to also have depths ranging from 10 ft to over 200 ft. Water depths across the map ranged from 0 ft (i.e., piezometer and surface and water samples) to a max of 365 ft, with some wells having depths as shallow as within 20 ft of the surface. Water table depths appeared generally shallower (<100 ft) in the O'Donnell Creek subwatershed, although this could be due to more samples being collected adjacent to rivers and streams in this area. There also appears to be a region of deeper water table depths (>200 ft) near the lower watershed, near the intersection of Highways 82 and 90. Water depths in the community of Elgin spanned the entire range of depths presented in the map. Montgomery & Associates and Natural Channel Design Engineering Inc. (2025) have a more detailed water table depth map that captures the entire watershed using a shaded relief diagram, rather than isolated point measurements as in *Figure 3.*

Stable Water Isotopes

All $\delta^{18}O_{H2O}$ and $\delta^{2}H_{H2O}$ values in this study are provided in *Table 2* and reported relative to the Vienna Standard Mean Ocean Water (VSMOW) standard; these values have also been plotted individually in *Figure 4a,* as well as being grouped together as trendlines by sampling location and sample type in *Figure 4b.* Samples from Stratman (2022) and Schwartzmann (1990) are included in both graphs.

Both *Figure 4a* and *4b* include several extra lines for reference, including a Global Meteoric Water Line (GMWL), Local Meteoric Water Line (LMWL), and San Pedro River evaporation trendline. The GMWL is given by the equation $\delta^{2}H = 8\delta^{18}O + 10‰$ (Craig, 1961). A true LMWL for the Babocomari Watershed could not be constructed due to a lack of long-term precipitation data in the area, so an estimated LMWL was instead plotted using modified Tucson basin precipitation data from Eastoe and Towne (2018)—a method also used by Stratman (2022). This LMWL was created by first identifying the average $\delta^{18}O$ and $\delta^{2}H$ values of winter precipitation (-9.5‰, -65.0‰) and summer precipitation (-6.2‰, -45‰) of the 30% wettest storms in the Tucson Basin (Eastoe and Towne, 2018). Given Elgin is at a higher elevation than the Tucson Basin, these SWI values then needed to be modified to account for the fact that $\delta^{18}O$ and $\delta^{2}H$ values of precipitation tend to decrease linearly with sampling altitude at a given "lapse rate" (Eastoe and Wright, 2019). Between Tucson and the Santa Catalina Mountains, every 1000m increase in altitude caused the $\delta^{18}O$ and $\delta^{2}H$ values of precipitation to decrease on average by -1.1 and -8.9‰ respectively in the winter, as well as by -1.6 and -7.7‰ in the summer (Eastoe and Wright, 2019). Since the average sampling elevation in Elgin was ~1450m above sea level, and Eastoe and Dettman (2016) reported an elevation of 753m to represent the Tucson Basin rain gages from which the winter and summer precipitation values were obtained, the calculated elevation increase of 697m between Tucson and Elgin was then used in tandem with the aforementioned altitude lapse rates to get new Elgin precipitation $\delta^{18}O$ and $\delta^{2}H$ values of -10.3 and -71.2‰ respectively in the winter, as well as -7.3 and -50.4‰ respectively in the summer. Drawing a line between these new summer and winter precipitation endmembers yielded the constructed LMWL shown in *Figure 4a* and *4b.* An evaporation line for the San Pedro River (given by the linear equation $\delta^{2}H = 3.6*\delta^{18}O - 27.4‰$) was also drawn in both of the aforementioned figures using data from Eastoe and Towne (2018) to see if any evaporation trends in the sampling data were reminiscent of Pattern 3 recharge along the San Pedro River.

In *Figure 4a*, groundwaters in the upper Watershed from Elgin tended to have higher SWI values relative to samples in the lower watershed and O'Donnell Creek subwatershed, with the bulk of Elgin samples falling between $\delta^{18}O$ values of -7 to -6‰, and $\delta^{2}H$ values of -55 to -45‰. Babocomari Cienega surface water samples from the middle Babocomari Watershed plotted even higher, with most falling between $\delta^{18}O$ values of -6.5 to -4‰ and $\delta^{2}H$ values of -45 to -35‰. Almost all of these samples exhibited an evaporation trend, plotting above and right of the LMWL.

The seasonality of recharge in these samples can be determined by tracing the trendlines in *Figure 4b* back to the LMWL. The upper Babocomari Watershed groundwater trendline traces back to a point between the summer and winter endpoints of the LMWL, indicating water in the Elgin area is recharged from a mix of local summer and winter precipitation, with its shallower slope and elevated SWI values relative to the LMWL indicating this recharge also experienced some evaporation. This mixing of recharge seasonality in addition to the presence of evaporation are both also exhibited in the groundwater data of the O'Donnell Creek subwatershed (Stratman, 2022). Although the middle Babocomari Watershed groundwater line appears to trace back closer to the winter precipitation endpoint, only four or five groundwater samples were collected in this area, so additional sampling might change this trend. On the other hand, the surface water samples from the middle Babocomari Watershed form a much clearer linear grouping in *Figure 4a* and *4b* that plots above the San Pedro River evaporation line and traces back to the summer precipitation endpoint of the LMWL, indicating water in the Babocomari Cienega primarily comes from evaporated summer recharge.

While these results go against the wider trend observed in the San Pedro watershed of groundwater primarily coming from winter recharge (Wahi, 2005; Hopkins et al., 2014), they agree with a point made by Montgomery & Associates and Natural Channel Design Engineering Inc. (2025) that regions of Arizona with intense summer monsoon precipitation like the Babocomari Watershed could receive more groundwater recharge and flow in ephemeral washes during the summer than during the winter which would explain the summer bias in the isotope ratios of the middle Babocomari Watershed surface water samples, as well as the more mixed seasonality of recharge elsewhere in the watershed.

Major Ion Chemistry and PCA

The field meter measurements and calculated total dissolved solids for all samples collected in this study are provided in *Table 3*, as well as their anion and cation concentrations in *Table 4a* and *4b*, respectively. Samples from all three collection areas (i.e., the upper Babocomari Watershed near Elgin, the middle Babocomari Watershed near the Babocomari Cienega, and the O'Donnell Creek subwatershed) were predominantly Ca-HCO_3 type waters. This trend of calcium-bicarbonate-type waters was also identified in Stratman's 2022 study along O'Donnell Creek, Schwartzmann's 1990 study in the lower Babocomari Watershed, and Hopkins et al.'s 2014 study in their mountain-block samples of the Middle San Pedro Watershed. This trend makes sense given the abundance of calcitic and carbonate sedimentary rocks in the region like limestones, as detailed in this report's **Site Description** section.

Figure 5, which includes samples from this study, as well as from Stratman (2022) and Schwartzmann (1990), shows additional evidence of the strong influence of carbonate minerals on the chemistry of waters in this region, with the bicarbonate (HCO_3^-) molar concentration of many samples being twice as high as their summed calcium and magnesium (Ca^{2+} and Mg^{2+}) molar concentrations, manifesting as a 1:2 linear trendline line on the graph. This occurs because bicarbonate ions only have a charge of negative 1, while calcium and magnesium ions have a charge of positive 2, meaning carbonate minerals (and the waters dissolving them) will have roughly twice as much bicarbonate as they do calcium and magnesium in order for their ionic charges to balance out. Also labeled on *Figure 5* are arrows showing carbonate dissolution and carbonate precipitation trends: waters not yet saturated with carbonate ions are capable of dissolving more carbonate minerals, which increases their ion concentrations; conversely, waters which have reached or exceeded saturation with carbonate ions will tend to exhibit decreases in their ion concentrations as the ions back-precipitate out of the water to form secondary carbonate minerals. Samples from O'Donnell Creek in *Figure 5* tended to have higher concentrations of all the aforementioned ions—plotting upwards and to the right on the graph, while samples from the upper and lower Babocomari Watershed tended to have lower concentrations—plotting downwards and to the left. Samples from the middle Babocomari Watershed plotted across the board, though more of these samples seemed to skew towards the high-concentration end, alongside the O'Donnell Creek samples.

To draw more concrete conclusions from these spatial trends, Principal Component Analysis (PCA) was performed to identify similarities in the ion concentrations between the middle Babocomari Watershed samples and samples from the two areas upstream (i.e., the O'Donnell Creek subwatershed and in the upper Babocomari Watershed near Elgin), with the results being plotted in *Figure 6;* samples from this study and from Stratman (2022) are included in this figure. As described in the **Methods** section, only those ions contributing significant variation to the data were included in the PCA analysis, being Na^{+}, Ca^{2+}, Mg^{2+}, and HCO_3^{-}. Since there are "p = 4" ions in this analysis, each principal component (PC) has to contribute at least "1/p = ¼ = 0.25 = 25%" of the variation in the dataset, with the two resultant Principal Component axes—PC1 and PC2—contributing 61.6% and 25.0% of the variation respectively. From this graph, the divergence in hydrochemistry between the upper and middle Babocomari Watershed is evident, with the upper Babocomari Watershed (Elgin) samples plotting mostly to themselves in the mid/upper left of the graph, and middle Babocomari Watershed samples plotting mostly within the cloud of O'Donnell Creek subwatershed samples, implying the hydrochemistry of the latter two areas are more similar to one another.

These similar chemistries could imply that the Babocomari Cienega receives more water from the O'Donnell Creek subwatershed than from the upper Babocomari Watershed near Elgin. Although this is initially counterintuitive considering the Babocomari River has its headwaters in Elgin, these results agree with the kriged water table map from *Figure 2*, where the groundwater contours imply water passing through the Elgin area would flow northeastwards towards the Mustang Mountains, while groundwaters in the O'Donnell Creek area would flow northeastwards towards the middle Babocomari River. The water table map from Montgomery & Associates and Natural Channel Design Engineering Inc. (2025) even shows that some water in Elgin actually flows northwestward and out of the Babocomari Watershed, further supporting the idea that the Elgin area does not contribute was much water to the Babocomari Cienega.

However, it is prudent to emphasize that the lack of hydrogeochemical data from other parts of the watershed like the Mustang Mountains and Huachuca Mountains makes it difficult to tell concretely whether the O'Donnell Creek subwatershed is the *primary* source of water to the Babocomari Cienega—only that this subwatershed contributes *more* water than the Elgin area. To that end, two well samples from the upper Babocomari Watershed, UG11 and UG13, were located close to the Mustang Mountains, and had measurements that stood apart from other samples in Elgin; specifically, compared to the bulk of Elgin samples, both UG11 and UG13 had lower SWI values, with UG11 also having the highest sodium concentration and lowest magnesium, potassium, and calcium concentrations of any sample in this study. (UG11 also had the lowest δ^{13}C-DIC value of all Elgin samples, which will be discussed in the next section). Although these two samples are not enough to make a robust PCA conclusion, they support the possibility that groundwaters near the Mustang Mountains may be chemically and/or isotopically distinct from Elgin waters. Additionally, it could be argued that the chemical similarity between the middle Babocomari Watershed waters and O'Donnell Creek waters may be explained by their similar environments—both containing Cienegas with areas of heavier vegetation when compared to the more sparsely vegetated Elgin area. The lack of flowing surface water in the upper Babocomari River throughout this study's sampling periods meant no surface water samples from the Elgin area can be used as comparison to surface waters along O'Donnell Creek and the middle Babocomari River, so collecting additional samples for a more detailed PCA would be a good prospect for future research.

δ^{13}C-DIC, Tritium, and Radiocarbon

δ^{13}C-DIC, tritium, and radiocarbon measurements are provided for this study's samples in *Table 5*. Most groundwater samples collected in this study had tritium at or below detection limits (BDL), meaning they had little to no modern recharge from after the 1950s. Three groundwater samples in Elgin (UG7a, UG8, UG9) had small but measurable tritium—1.1 to 1.3TU—implying they contain a component of modern recharge. The groundwater sample with the highest tritium was MG2a with 2.8TU, which makes sense considering the well this sample came from was likely being fed by a large pond directly adjacent to it within the Babocomari Cienega, as evidenced by the well's shallow water depth of 29 ft as indicated by its well logs, as well as the fact that many surface water samples along the middle Babocomari Watershed had tritium levels at or above 3TU. A spring in O'Donnell Creek was sampled twice for tritium and measured BDL both times, implying it was fed by groundwater that received no modern precipitation inputs. Three surface water samples in the same O'Donnell Creek area (two at a river flowing over a dam and one at the same river but upstream) had tritium levels from 1.3 to 2.1 TU—slightly lower than the middle Babocomari Watershed surface water samples. This could imply the middle Babocomari Watershed surface water samples are fed by a larger component of modern precipitation which tends to have tritium levels between 3 and 5 TU (University of Arizona Environmental Isotope Laboratory, 2022).

Radiocarbon of dissolved inorganic carbon was only analyzed in groundwater samples since surface waters were assumed to already be equilibrated with atmospheric CO_2. Ten well water samples (nine from the upper Babocomari Watershed and one from the middle Babocomari Watershed) were analyzed for radiocarbon. After performing age corrections on them using the Han and Plummer (2013) spreadsheet, all ten samples' corrected radiocarbon ages were submodern (<500 years old). This initially seemed counterintuitive, as most of the upper Babocomari Watershed samples had elevated δ^{13}C-DIC values typically above -7‰, while O'Donnell Creek samples from Stratman (2022) were typically less than -7‰; this divergence is depicted in *Figure 7*, which plots the δ^{13}C-DIC values of the samples against their tritium values. As described in the **Background on Major Environmental Tracers** section, higher δ^{13}C-DIC values are typically associated with older waters that have spent more time dissolving high-δ^{13}C-DIC carbonate minerals. As such, the higher δ^{13}C-DIC values of the upper Babocomari Watershed samples might normally imply they should be older than samples in the O'Donnell Creek area, yet the prevalence of corrected radiocarbon ages below 500 years old in the upper Babocomari Watershed matches the typical age range seen in the O'Donnell Creek dataset of Stratman (2022).

These results are further complicated by the process of incongruent carbonate dissolution, wherein waters reaching saturation with carbonate minerals begin to back-precipitate calcite, resulting in a characteristic trend of decreasing alkalinity/bicarbonate concentration with increasing δ^{13}C-DIC values—a trend previously observed in both the Cienega Creek watershed to the north (Vicenti, 2018), as well as in the O'Donnell Creek subwatershed by Stratman (2022). Not only is this trend indeed also observed in samples from the upper Babocomari Watershed in *Figure 8,* but confoundingly, the upper Babocomari Watershed samples clearly exhibit lower HCO_3^- and higher δ^{13}C-DIC than samples from the O'Donnell Creek area, implying more incongruent carbonate dissolution has taken place and thus suggesting the upper Babocomari Watershed should indeed have older waters. However, even sample UG2 with the lowest radiocarbon value of 16.92pMC and the highest δ^{13}C-DIC value of -1.4‰ still produced a corrected radiocarbon age below 500 years old.

An additional problem was the loss of four radiocarbon samples from sites UG6a, UG10a, MG1, and MG2a due to their breakage during shipment to the radiocarbon lab. Although these sites were later revisited with the intent to recollect their radiocarbon samples, funding limitations at that point in the project necessitated more scrutiny with regards to what samples could be analyzed. It was later decided not to analyze these recollected radiocarbon samples, since UG6a, UG10a, and MG1 had similar $\delta^{13}C$-DIC values to other samples from this study whose corrected radiocarbon ages already turned up submodern, and MG2a likely would have also turned up submodern since it was identified earlier as likely receiving water from the nearby Babocomari Cienega, whose surface waters would have already equilibrated with atmospheric radiocarbon. As such, the remaining funding was instead directed towards analyzing sample UG11 from Elgin due to its uncharacteristically low $\delta^{13}C$-DIC value of -10.1‰—distinctly the lowest of any sample from the upper Babocomari Watershed and putting it more in the range expected from an O'Donnell Creek sample. However, this sample, too, ended up having a submodern corrected radiocarbon age like the rest of the samples from Elgin.

Nitrate Concentrations and Isotopes

All of the surface water samples collected along the middle Babocomari Watershed, in addition to all of the samples from the O'Donnell Creek area collected in this study had nitrate concentrations below 1 mg/L, with many falling below nitrate's detection limit of 5µmol/L (~0.31 mg/L). The three groundwater wells sampled in the middle Babocomari Watershed (MG1, MG2, and MG3) had slightly higher nitrate concentrations of 2.56, 3.46, and 5.84 mg/L respectively, with only the latter well (MG3) exceeded the typical background nitrate level of 4.5 mg/L (Dubrovsky et al. 2010), although these concentrations are still relatively low.

Of the thirteen groundwater wells sampled in the upper Babocomari Watershed near Elgin, eight fell below the background nitrate level of 4.5 mg/L, three had slightly higher concentrations between 5.01 and 8.38 mg/L, and two had notably elevated nitrate concentrations of 17.89 mg/L (UG1a) and 52.37 mg/L (UG7a) with the latter exceeding the EPA's nitrate maximum contaminant level (MCL) of 45 mg/L. These two wells with high nitrate concentrations were originally sampled in 2023, and upon resampling them for nitrate isotopes in 2024 to determine where their nitrate was coming from, both exhibited decreases in their nitrate concentrations, with UG1b at 13.90 mg/L and UG7b at 34.21 mg/L.

One method used to get an idea of the nitrate source at these wells involved graphing their NO_3^-/Cl^- molar ratios against their chloride concentrations. Data from a study by Gibrilla et al. (2020) using borehole wells, hand-dug wells, and surface water samples in Ghana, Africa showed that waters contaminated by manure/septic nitrate sources tend to have lower NO_3^-/Cl^- molar ratios and higher chloride concentrations, while waters contaminated by fertilizer nitrate tend to have higher NO_3^-/Cl^- molar ratios and lower chloride concentrations. This relationship is graphed in *Figure 9a*, wherein the UG7a sample plots towards the middle-right of the graph, alongside a well sample that Stratman (2022) collected in the O'Donnell Creek area which was later found to be located near a leaky septic tank. While the location of these two samples in *Figure 9a* aligns with a septic contamination trend of lower NO_3^-/Cl^- molar ratios and higher chloride concentrations, the other samples—UG7b and UG1a/b—are less conclusive, plotting towards the middle/left of the graph, although with higher chloride concentrations than the bulk of samples. However, it should be noted that samples from the Gibrilla et al. (2020) study tended to have a much higher range of NO_3^-/Cl^- and chloride concentration values, so this graph has been rescaled in *Figure 9b* to match the range of samples from the Gibrilla et al. (2020) study. Here, the distinction in wells with possible manure/septic contamination is made a bit clearer, and in particular, two samples from Schwartzman (1990) are now labeled on the graph which had very elevated chloride concentrations. While Schwartzmann's lower Babocomari Watershed sample labeled on this graph had 61 mg/L Cl^- but only 0.2 mg/L NO_3^-, his upper Babocomari Watershed sample had 160 mg/L Cl^- and 37.2 mg/L NO_3^-; he suggested the anomalous elevated chloride could be due to septic contamination or inaccurate data (Schwartzmann, 1990).

A more conclusive way to identify the source of elevated nitrate in wells UG1 and UG7 is through nitrate isotope analysis. Kendall (1998) created a plot of $\delta^{15}N_{NO3}$ and $\delta^{18}O_{NO3}$ ranges typically expected from different nitrate sources, including natural sources like precipitation and soil nitrogen, as well as anthropogenic sources like fertilizers and manure/septic contamination; this plot is included in the nitrate isotope graph of *Figure 10*, with the nitrate isotope values from *Table 6* for UG1b ($\delta^{15}N_{NO3}$ = 12.3‰ AIR and $\delta^{18}O_{NO3}$ = 9.8‰ VSMOW) and UG7b ($\delta^{15}N_{NO3}$ = 8.3‰ AIR and $\delta^{18}O_{NO3}$ = 1.1‰ VSMOW) in 2024 overlain on this graph. Both samples fall clearly into the manure/septic nitrate isotope range, which spans $\delta^{15}N_{NO3}$ values of roughly 0 to 25‰ AIR and $\delta^{18}O_{NO3}$ values of roughly -5 to 15‰ VSMOW. Although UG7b also falls just on the border of the soil nitrogen range in *Figure 10* (which overlaps the manure/septic range), the concentration of nitrate at the UG7 site in both 2023 and 2024 is still nonetheless higher than would be expected of natural soil nitrogen, further supporting the idea of the well having manure/septic contamination.

The comparably high nitrate concentrations at UG7 and Stratman's O'Donnell Creek sample (compared to the relatively lower nitrate concentration at UG1) could be explained be the amount of modern recharge that the different sites received, which can be determined from their tritium concentrations as depicted in *Figure 11.* While UG1 had tritium below detection limits, UG7 and Stratman's sample had at least 1TU, so their comparably higher nitrate could be a result of these wells having a component of modern recharge which makes them more susceptible to modern sources of contamination. This agrees with the global trend of wells with tritium levels above 0.8TU being more likely to have elevated nitrate concentrations compared to wells with less tritium (Jasechko, 2019).

Transpiration

Figure 12 plots the chloride concentration of each sample against their $\delta^{18}O_{H2O}$ value. Samples in this figure include those collected in this study, as well as samples from Schwartzman (1990) and Stratman (2022). The piezometer samples that Stratman (2022) collected along O'Donnell Creek exhibit a trend of increasing chloride concentration with little change in $\delta^{18}O_{H2O}$, which Stratman identified as a transpiration trend. This is consistent the transpiration trend that Wahi (2005) identified in the Upper San Pedro Watershed. While such a transpiration trend is not visible in the middle Babocomari Watershed surface water samples in *Figure 12*, the lack of shallow piezometer samples along the Babocomari Cienega and River means it is difficult to determine the extent of transpiration in the middle Babocomari Watershed from this graph. To avoid misinterpretation, three wells have been labeled on *Figure 12* and noted as having elevated chloride due to septic contamination, rather than transpiration.

Seasonal Changes in Surface Water and Anomalous Babocomari Cienega Sample

A handful of surface waters sites along the Babocomari Cienega and O'Donnell Creek Cienega were sampled in April of 2024 and then again in November of 2024 to try capturing any seasonal variability in their measurements before versus after the 2024 summer monsoon season. These included: OS1b/OS2, OR1b/c, MS4a/b, and MS7a/b. Upon returning to the Babocomari

Watershed in November of 2024, numerous residents in the area reported via in-person correspondence that the monsoon that year was unusually dry; additionally, many of the revisited surface water sites either had noticeably lower water levels than in April or had gone dry entirely.

OS1b/OS2 was one set of sampling sites affected by this dryness, as OS1b was originally collected from river water in O'Donnell Creek flowing over a small dam in April; this portion of the river had gone dry by November, so the post-monsoon sample (OS2) was instead collected from the river roughly 600 feet upstream of the dam where it was still flowing. Comparing the two samples, all of its ion concentrations had decreased slightly from April to November, and its tritium dropped from 2.1 to 1.3 TU, with its other measurements remaining mostly the same. It is possible this lack of significant change in this sample's measurements was a result of the dryness of the monsoon season that year, meaning there would not have been enough monsoon precipitation input to significantly affect the sample's chemistry. A spring water site from the same area—OR1b/c—was flowing both before and after the monsoon season and exhibited little to no change in all of its measurements between sampling periods; in this case, a more pertinent explanation for the lack of measurement change could be the fact that since this is a spring fed by submodern regional groundwater (as evidenced by the sample's BDL tritium), it would be less affected by changes in modern precipitation inputs.

MS4a/b was located along the Babocomari River and was also technically two different sampling sites, since the section of river sampled in April as MS4a had gone dry by the time November arrived; the river was still flowing 200 ft upstream, so the post-monsoon sample was collected at this upstream site and given a similar name—MS4b—since the two locations were within eyesight of one another. This sampling area, too, exhibited little change in its measurements before versus after the monsoon, which—like with the OS1b/OS2 site—may again be explained by the dry monsoon limiting the influence of summer rains.

The only site to show particularly anomalous changes in its measurements after the monsoon season was MS7a/b, a surface water sample collected at a large, vegetated pond within the Babocomari Cienega. This was the same pond adjacent to well MG2, as described in the previous sections. The pre-monsoon surface water sample at this pond had a tritium level of 0.6TU—almost at the minimum detection limit—which initially made it seem like the pond was fed by a spring. However, after the monsoon season, the pond's tritium level shot up to 7.8TU—the highest of any sample from this study and even exceeding a 2021 summer precipitation sample from Stratman (2022) which had 5.4TU—the highest of any sample in his study. The pond's post-monsoon sample also had stark decreases in almost all of its ion concentrations, with some dropping to almost half the level of their pre-monsoon counterparts. Lastly, the pond's $\delta^{18}O_{H2O}$ and $\delta^{2}H_{H2O}$ values spiked from -5.2 and -40.6‰ pre-monsoon to -2.1 and -20.9‰ post-monsoon, making the post-monsoon sample the highest-SWI sample of this dataset, as well as the highest in the datasets of Schwartzmann (1990) and Stratman (2022) (excluding an anomalous cattle stock tank sample from the latter). Though there are a few explanations for the unusual behavior at this site, each explanation seems to conflict with one another. For example, the decrease in ion concentrations combined with the stark increase in tritium could imply an anomalous storm event with an uncommon moisture source fed a lot of water into the pond between the two sampling periods—enough to dilute the pond's chemistry. However, this goes against the aforementioned reports and visual confirmation of a dry monsoon season that year. Additionally, unless said anomalous storm was very localized, any storm large enough to change the chemistry of the entire pond would have also caused a more noticeable change in the measurements of the river downstream of the pond at MS4a/b, which was not observed. Leaning more into the dry monsoon aspect, one could argue that large increase in SWI values at this site could be explained by an evaporation trend, yet any evaporation significant enough to raise the SWI values of the entire pond should have coincided with an increase in the ion concentrations of the pond, yet the ion concentrations decreased across the board in the post-monsoon sample. The owners of the property on which the pond was located also confirmed that they did not do any water remediation activities that would have affected the water's chemistry, so unless additional samples can be collected in the pond at different times of year to see if the anomalous measurements are repeatable, an explanation has yet to be found for this site's behavior.

Conclusions

Stable water isotope data indicates Elgin groundwater comes from a mix of local summer and winter precipitation which has experienced evaporation, which agrees with trends from the O'Donnell Creek subwatershed, but which goes against trends in the wider San Pedro watershed of groundwater primarily coming from winter recharge. Surface waters along the middle Babocomari Watershed appear to come primarily from evaporated summer precipitation.

PCA implies waters along the Babocomari Cienega are more chemically similar to waters in the O'Donnell Creek subwatershed than waters along the upper Babocomari River near Elgin, which could indicate the Cienega receives more water from the former than the latter. However, the PCA could benefit from sampling in other areas that drive groundwater flow towards the Cienega, like the Mustang Mountains and Huachuca Mountains.

Radiocarbon dating shows Elgin groundwaters are mostly submodern (<500 years old), which agrees with results from Stratman (2022) in the O'Donnell Creek area, although this result is counterintuitive since elevated $\delta^{13}C$-DIC values in Elgin groundwater normally implies these waters should be older than O'Donnell Creek groundwaters. Three groundwater samples in Elgin had measurable tritium, implying mixing with modern recharge from after the 1950s. One groundwater sample from the middle Babocomari Watershed was also submodern and its tritium level was barely at the detection limit, implying it contained almost no modern recharge component. Babocomari Cienega surface waters have higher tritium levels relative to O'Donnell Creek surface waters, implying they are fed by a larger component of modern precipitation.

Nitrate isotope analysis revealed that two Elgin wells with elevated nitrate concentrations had manure/septic contamination. One of these wells had detectable tritium, implying it contained a component of modern recharge that made it vulnerable to modern contamination sources.

Future Research

Further hydrogeochemical research in the Babocomari Watershed would benefit from the development of a true LMWL through collecting long-term precipitation isotope data in the region. Additional sampling in both the Mustang Mountains and the Huachuca Mountains would also help identify with more certainty where most of the water feeding the Babocomari Cienega comes from via PCA, as well as the Cienega's susceptibility to modern anthropogenic influences, although sampling in these areas will likely be limited by accessibility and the availability of wells. Collecting more age tracer samples, like tritium, radiocarbon, and $\delta^{13}C$-DIC from groundwaters in the middle and lower Babocomari Watershed would further help round out data gaps, particularly with providing a wider spatial context to the evolution of groundwater ages through the watershed that may help explain the unusual incongruent carbonate dissolution behavior observed in the upper Babocomari Watershed. Collecting additional samples at the MS7 Babocomari Cienega pond site at different times of year could help illuminate the water sources feeding the area and explain its anomalous changes in isotopes and chemistry before versus after the monsoon season. Lastly, a safe yield value should be calculated in Elgin to determine the sustainability of groundwater withdrawal in the upper Babocomari Watershed.

Appendices

Appendix A – Figures

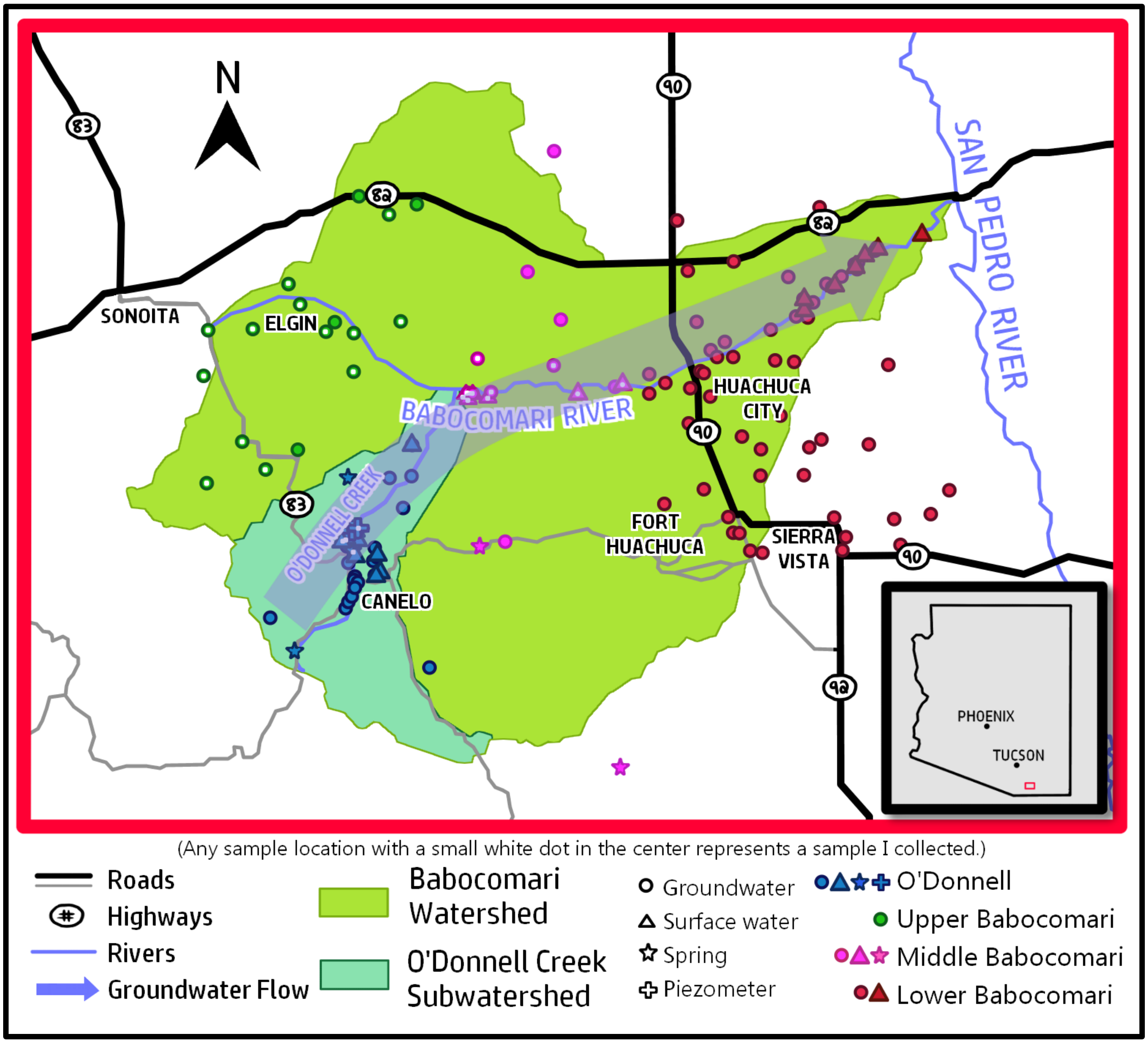

Figure 1a: Location of the Babocomari Watershed study area and sampling sites colorized by general watershed location. This plot includes samples that were collected for this study (indicated by sampling sites with white dots inside them), as well as samples from Schwartzmann (1990) who generally collected samples in the lower Babocomari Watershed, and Stratman (2022) who generally collected samples along O'Donnell Creek near Canelo.

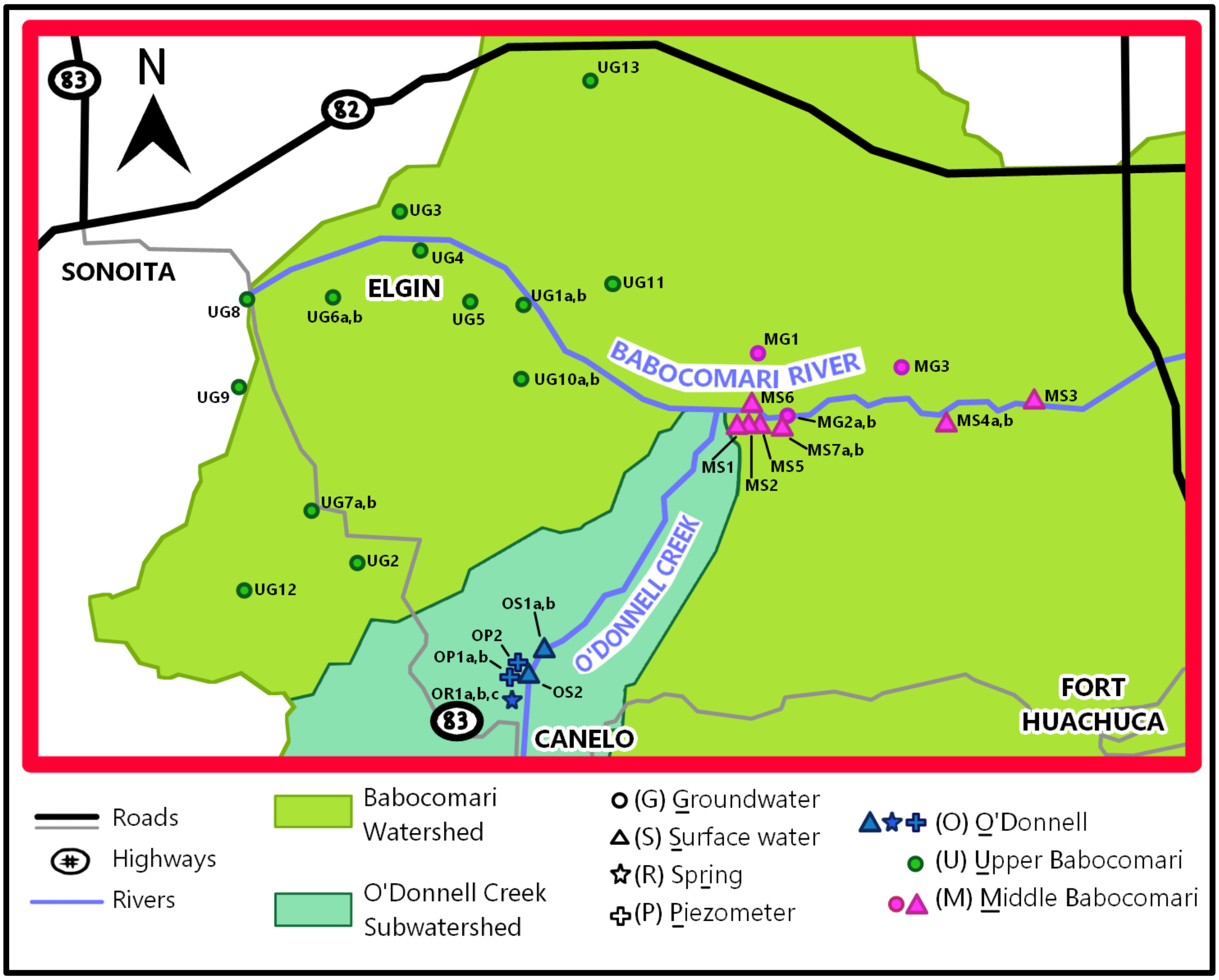

Figure 1b: Map of sites sampled for this study with IDs labeled. This map is the same map from Figure 1a but zoomed in, with only this study's samples shown. The sample ID indicates the sample's location (U = Upper Babocomari Watershed = U, M = Middle Babocomari Watershed, O = O'Donnell Creek subwatershed) and type (G = Groundwater, S = Surface water, P = Piezometer, R = Spring). Some sampling sites were sampled multiple times on different dates, as indicated by an "a", "b", or "c" after their sample ID.

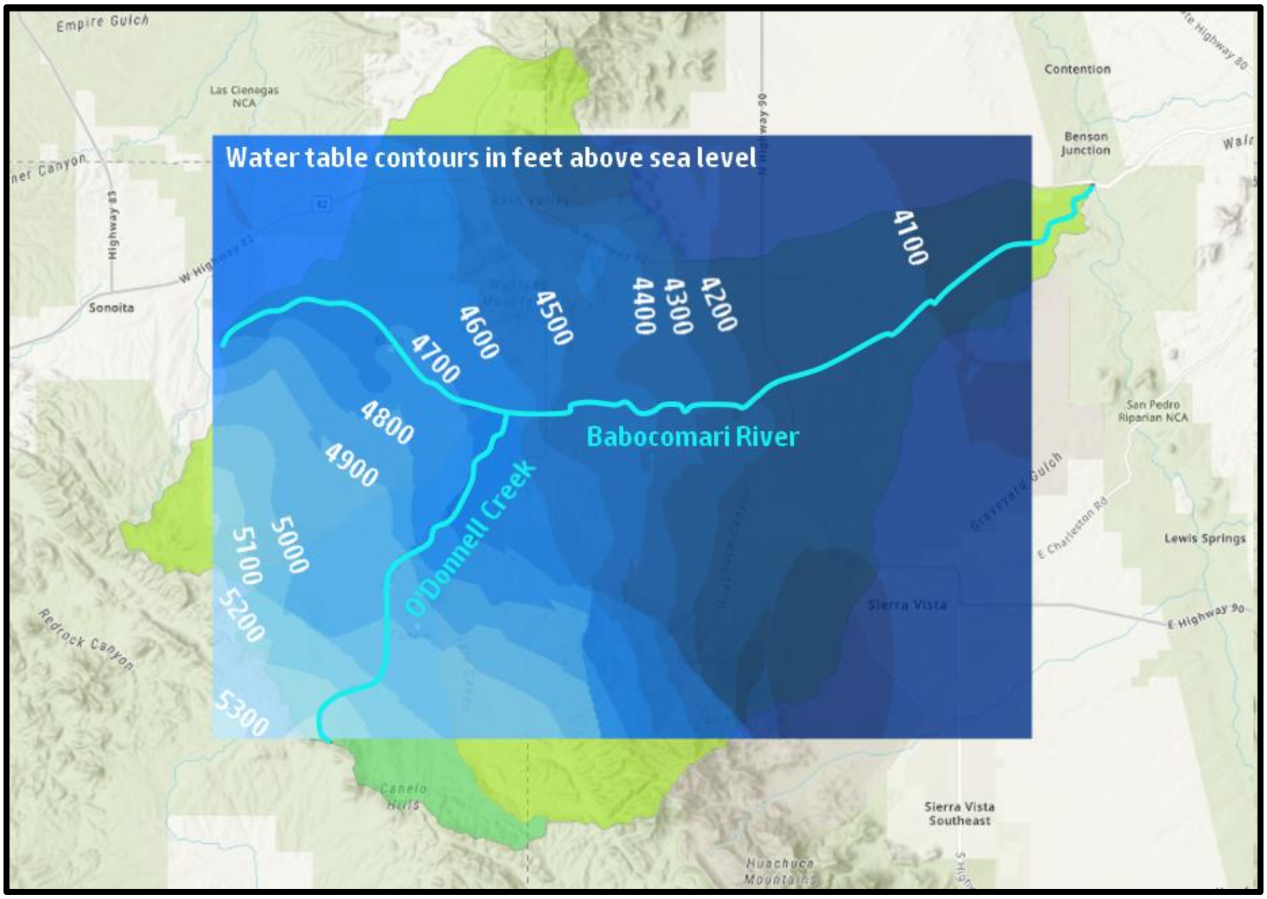

Figure 2: Kriged water table elevation map of the Babocomari Watershed in units of feet above sea level. Elevation data were obtained from in-situ GPS measurements for this study, as well as from Schwartzmann (1990) and Stratman (2022). Depth-to-water data was obtained at these locations from Wells 55. The Babocomari River and O'Donnell Creek are highlighted in cyan. Note that the accuracy of this map is limited by the number and location of samples collected, so areas with fewer samples (e.g., northern Babocomari Watershed near the Mustang Mountains and southern Babocomari Watershed near the Huachuca Mountains) may be less accurate.

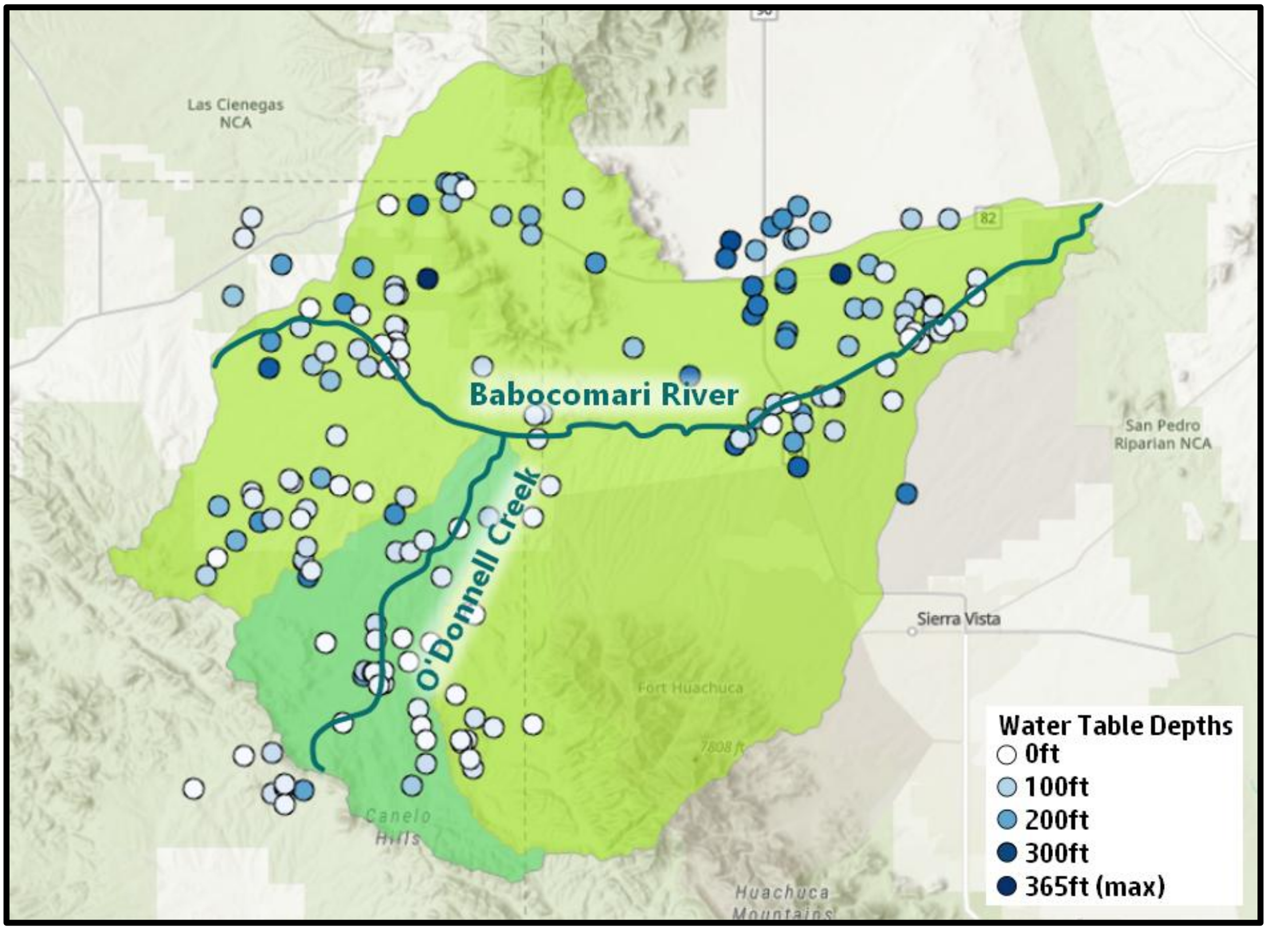

Figure 3: Map of point water table depths below the ground surface in feet in the Babacomari Watershed. The legend shows example depths in 100 ft intervals, up to a max depth of 365 ft. Well drilling dates and/or the dates of depth measurements were not taken into consideration in the creation of this map. Data were obtained from Wells 55, meaning this map includes many additional wells not sampled in this study, nor by Schwartzmann (1990) nor Stratman (2022).

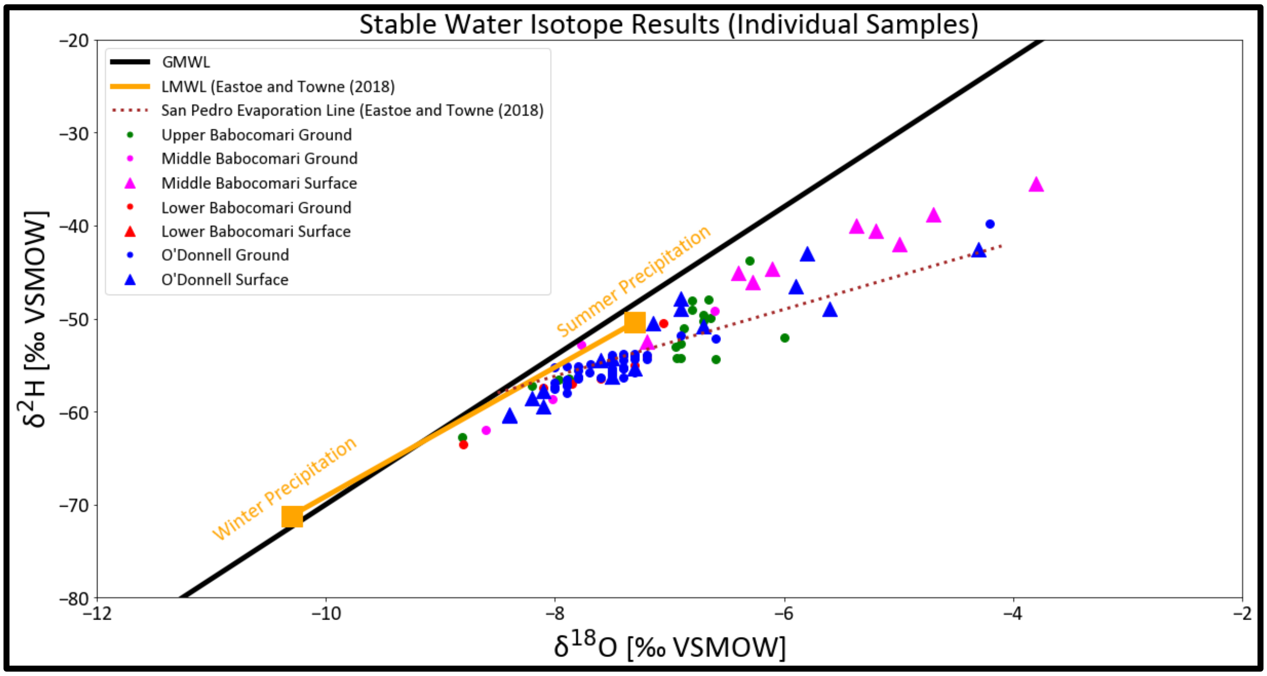

Figure 4a: Stable Water Isotope results for individual samples color-coded by sampling area, with a LMWL, GMWL, and San Pedro River Evaporation Line provided for reference. Samples from this study, as well as from Stratman (2022) and Schwartzmann (1990), are included in this graph. Groundwater from Elgin (upper Babocomari Watershed, green circles) appears to come from local winter and summer precipitation, while surface waters in the Babocomari Cienega (middle Babocomari Watershed, pink triangles) reflect evaporated local summer precipitation. The anomalous MS7b sample has been omitted from this graph.

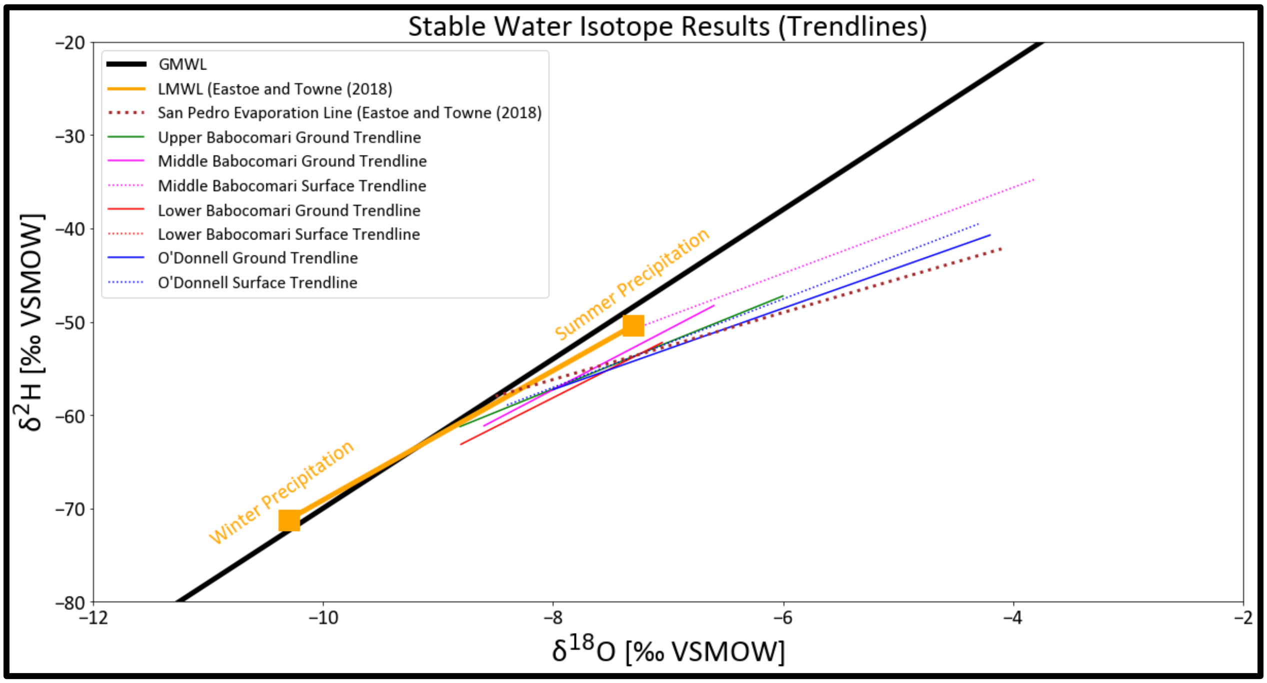

Figure 4b: Stable Water Isotope results plotted as trendlines and differentiated by region and sample type (groundwater vs surface water). Samples from this study, as well as from Stratman (2022) and Schwartzmann (1990), are included in this graph. A LMWL, GMWL, and San Pedro River Evaporation Line are provided for reference. The anomalous MS7b sample has been omitted from this graph.

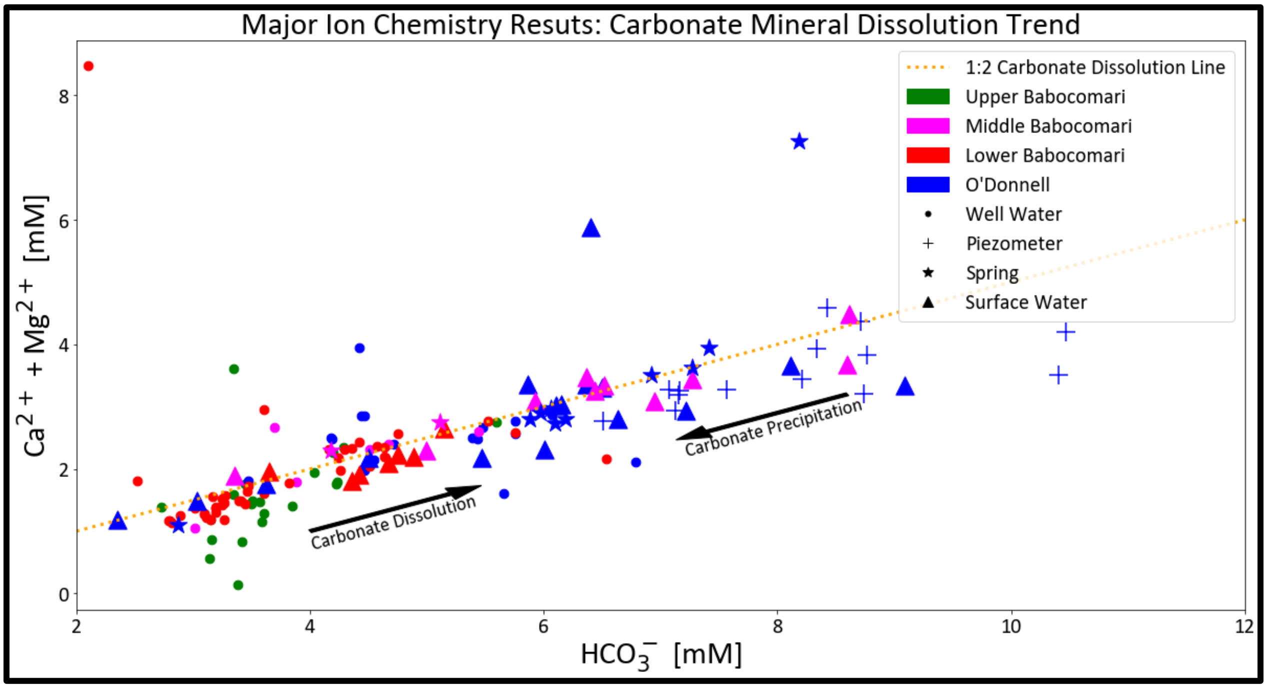

Figure 5: Carbonate mineral dissolution trend manifesting as a linear 1:2 trend between calcium plus magnesium molar concentration and bicarbonate molar concentration. Samples from this study, as well as from Stratman (2022) and Schwartzmann (1990), are included in this graph. O'Donnell Creek samples (blue) plot with higher concentrations (upwards and to the right) while samples from Elgin (green) plot with lower concentrations (downwards and to the left). Although samples from the middle Babocomari Watershed (pink) seem to plot along the entire range of concentrations, they skew more towards the higher concentration end, alongside the O'Donnell Creek samples.

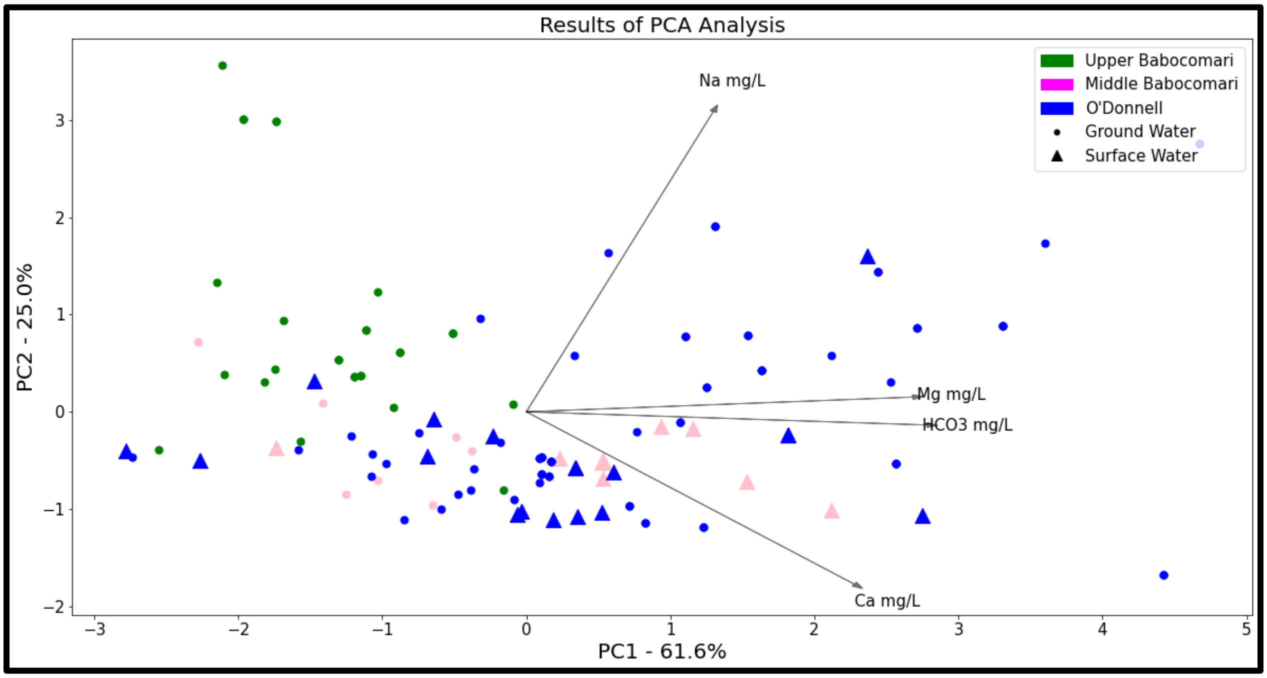

Figure 6: PCA scatterplot comparing the chemistries of middle Babocomari Watershed samples with samples from the upper Babocomari Watershed and O'Donnell Creek subwatershed. Samples from this study, as well as from Stratman (2022), are included in this graph. Vectors showing the principal ions used in this analysis and their relative contributions to PC1 and PC2 are also plotted. The upper and middle Babocomari Watershed samples appear to group separately from one another, with the middle Babocomari Watershed samples plotting more within the grouping of the O'Donnell Creek samples.

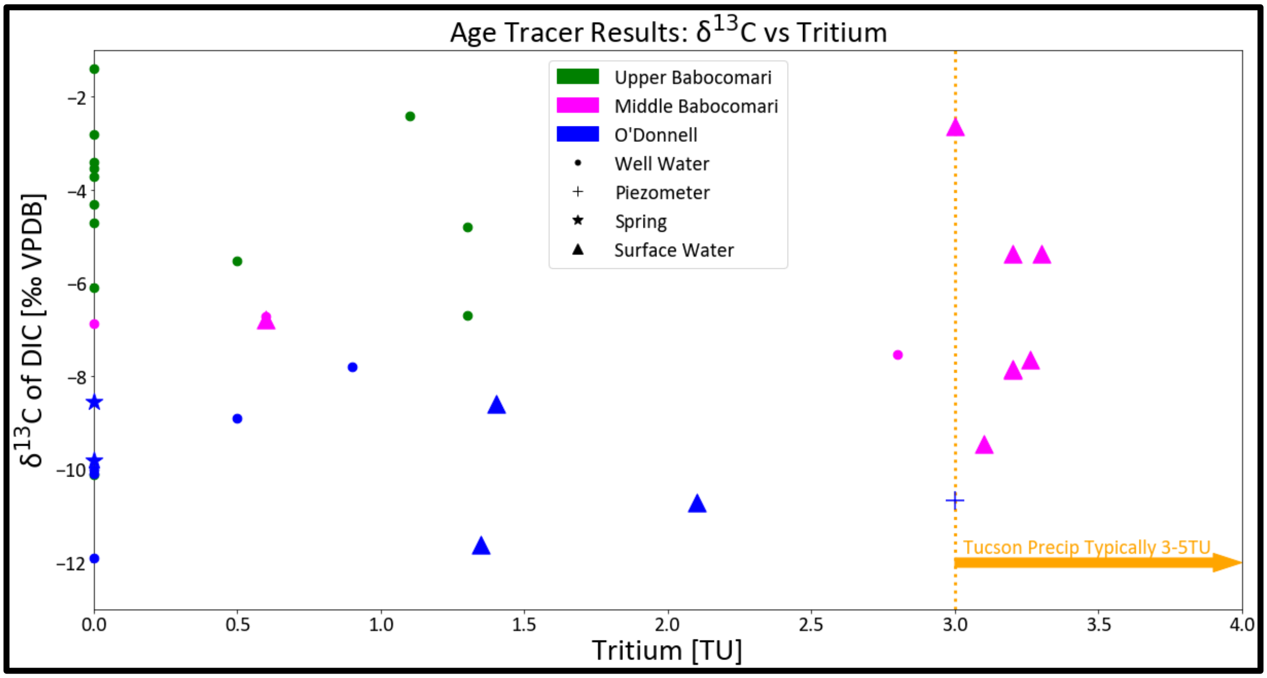

Figure 7: Plot of δ^{13}C-DIC vs Tritium showing divergence in δ^{13}C-DIC values between upper Babocomari Watershed samples and O'Donnell Creek samples, as well as the elevated tritium in middle Babocomari Watershed samples. Samples from this study, as well as from Stratman (2022), are included in this plot, as well as a yellow line and arrow showing the typical levels of tritium in precipitation via the University of Arizona Environmental Isotope Laboratory (2022).

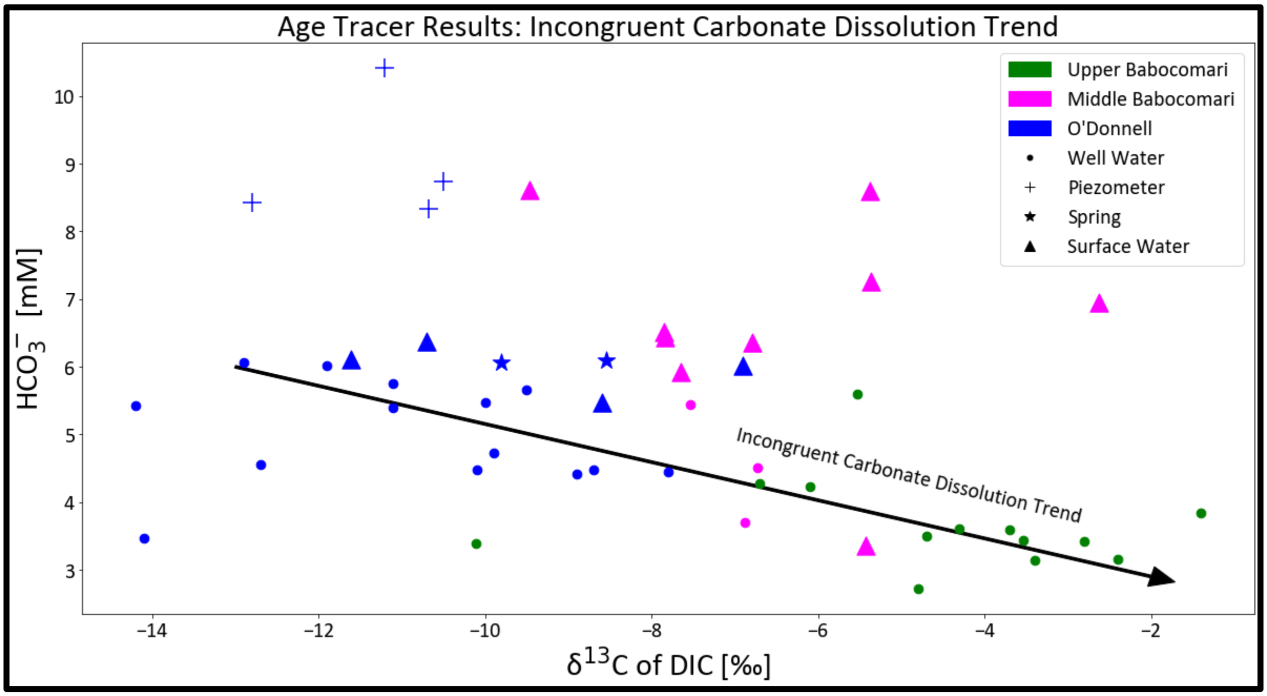

Figure 8: Plot of bicarbonate alkalinity versus δ^{13}C-DIC showing a trend of decreasing alkalinity with increasing δ^{13}C that is indicative of incongruent carbonate dissolution. Samples from this study, as well as from Stratman (2022), are included in this graph.

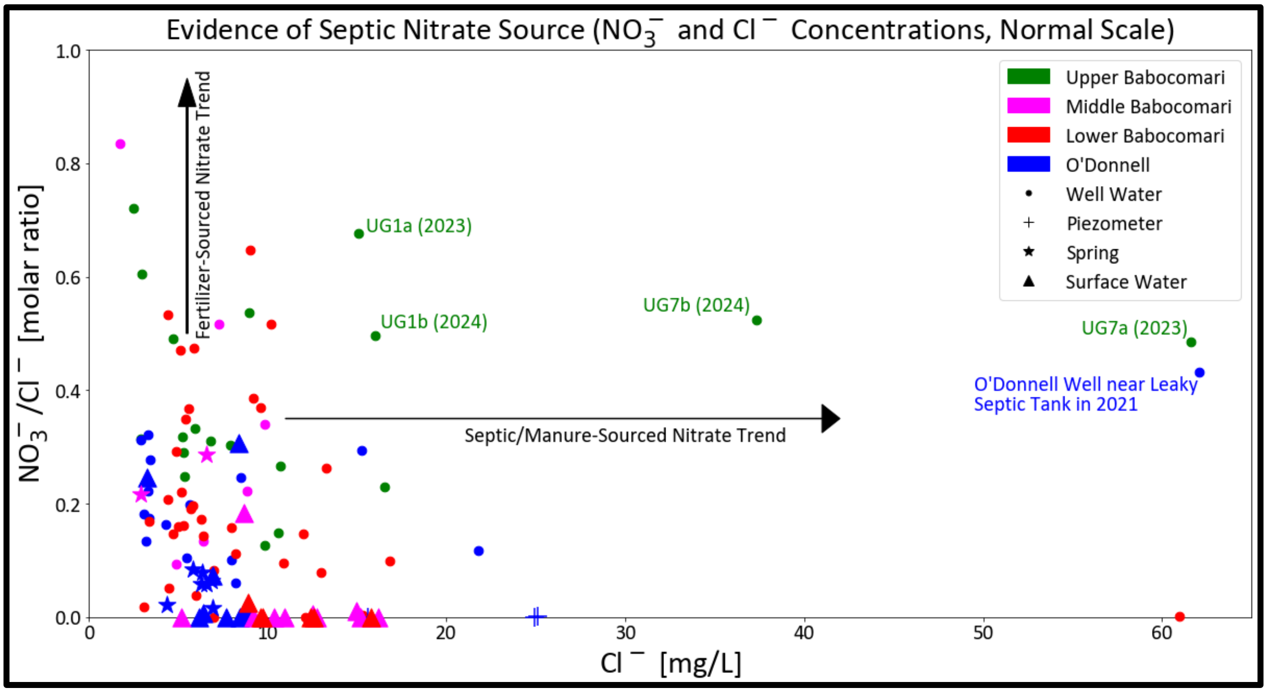

Figure 9a: Plot of NO_3^-/Cl^- molar ratio vs chloride concentration, with axes scaled to match the range of samples from this study, as well as samples from Stratman (2022), and Schwartzmann (1990). Gibrilla et al. (2020) notes that nitrate contamination from sewage or manure tends to have higher chloride concentrations and lower $NO3^-/Cl^-$ molar ratios. The O'Donnell Creek subwatershed well near the leaky septic tank in 2021 follows this trend, as does UG7 in Elgin in 2023 and 2024. Although UG1 does not follow this trend, it is still on the higher end of chloride concentrations for wells in Elgin.

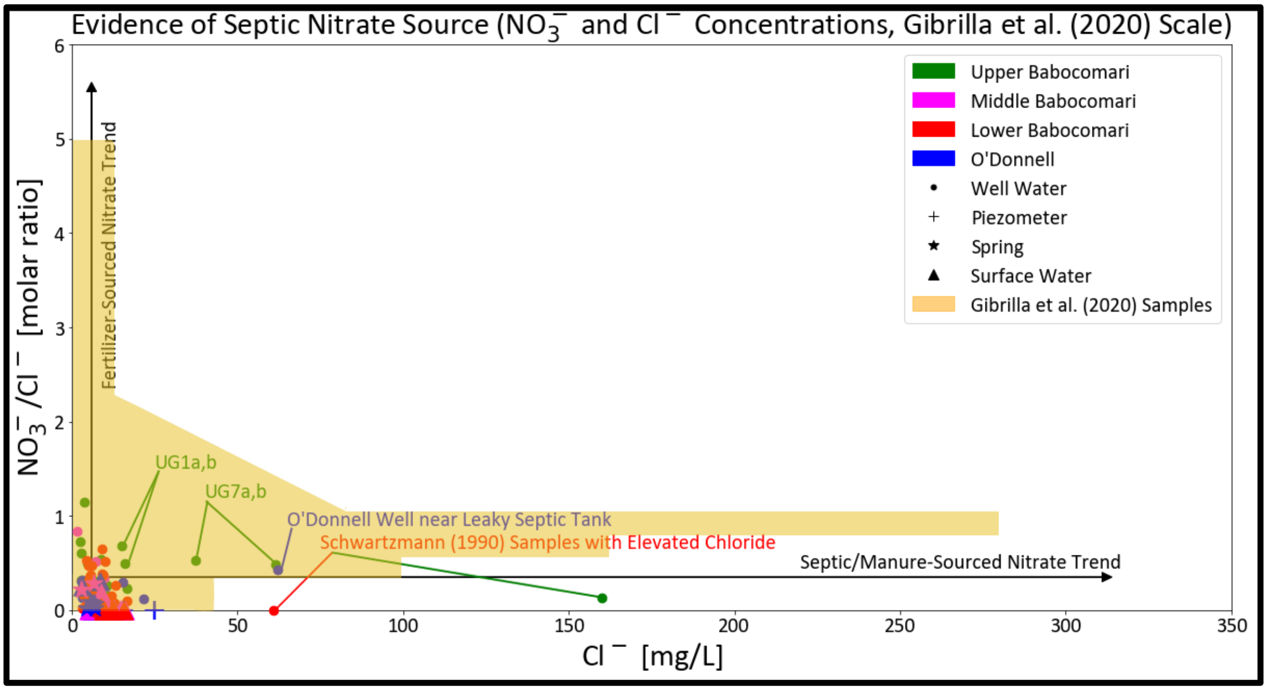

Figure 9b: Same NO_3^-/Cl^- vs chloride concentration graph as from Figure 9a, except now scaled to match the range of samples collected by Gibrilla et al. (2020) to give a better indication of what the different nitrate trends look like. Here, two Schwartzmann (1990) samples with elevated chloride are also labeled; Schwartzmann suggested the elevated chloride in his samples could be due to septic contamination, although only his upper Babocomari Watershed sample had high nitrate (37.2 mg/L), while his lower Babocomari Watershed sample had 0.2 mg/L nitrate.

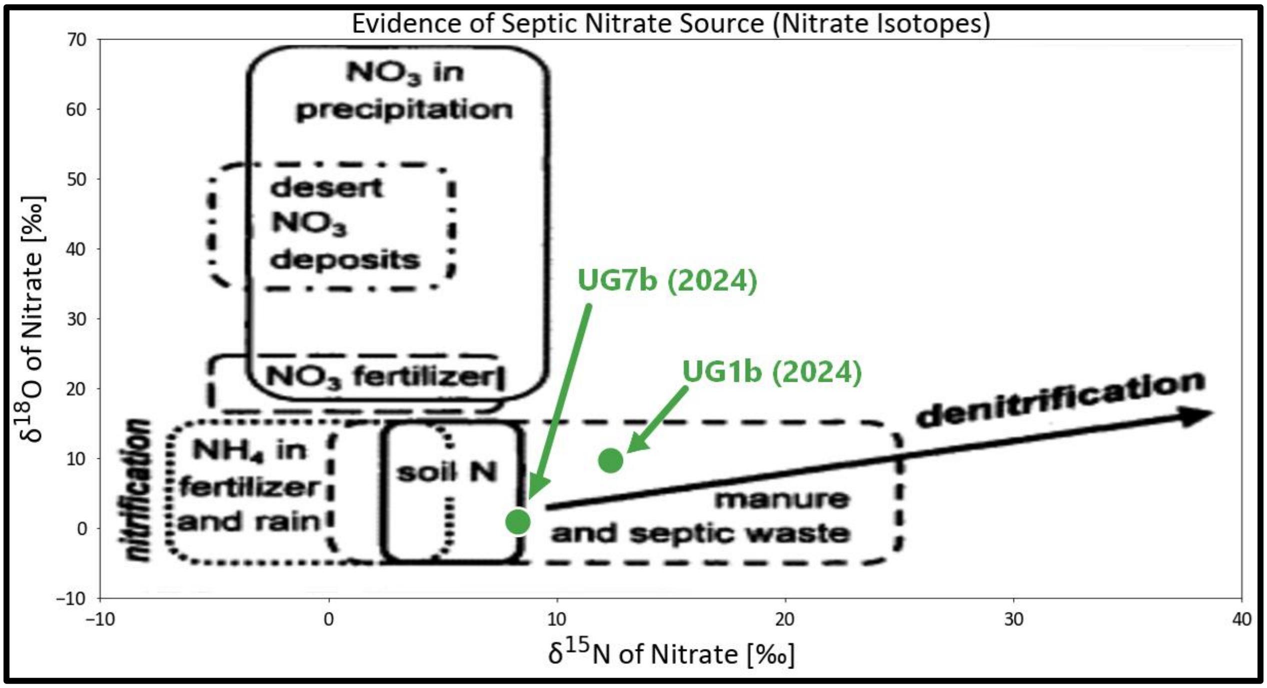

Figure 10: Nitrate isotope analysis showing how the two upper Babocomari Watershed samples with elevated nitrate in 2024 had nitrate isotope signatures consistent with manure and septic waste contamination, with leaky septic tanks being a known problem in rural areas lacking centralized sewage infrastructure. The background graph showing the isotope ranges expected from different nitrate sources is originally from Kendall (1998).

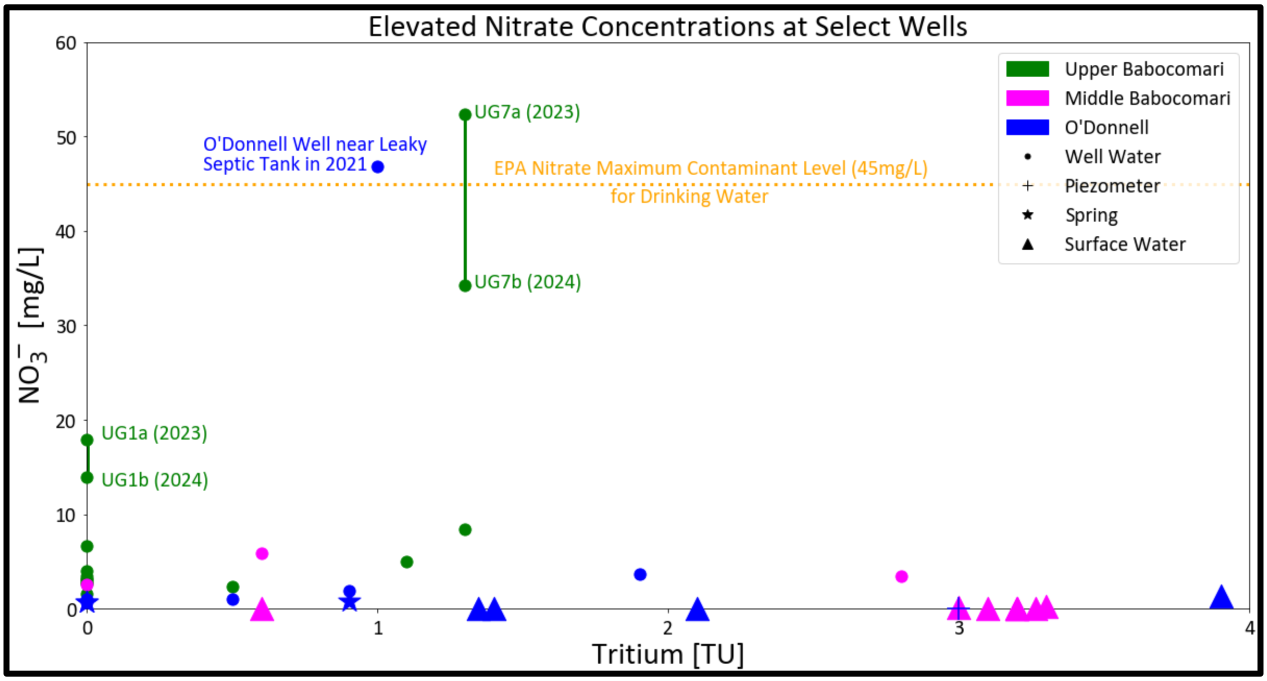

Figure 11: Nitrate versus tritium graph showing how some wells with elevated nitrate (e.g., Stratman (2022)'s Canelo well near a leaky septic tank and this study's UG7 sample) also had nonzero tritium, implying a component of modern recharge. Both UG1 and UG7 had their nitrate concentrations measured in 2023 and 2024, but their tritium levels were only measured in 2023, so a vertical line is used in the graph above to indicate that their 2023 and 2024 nitrate concentrations were both graphed against their 2023 tritium levels.

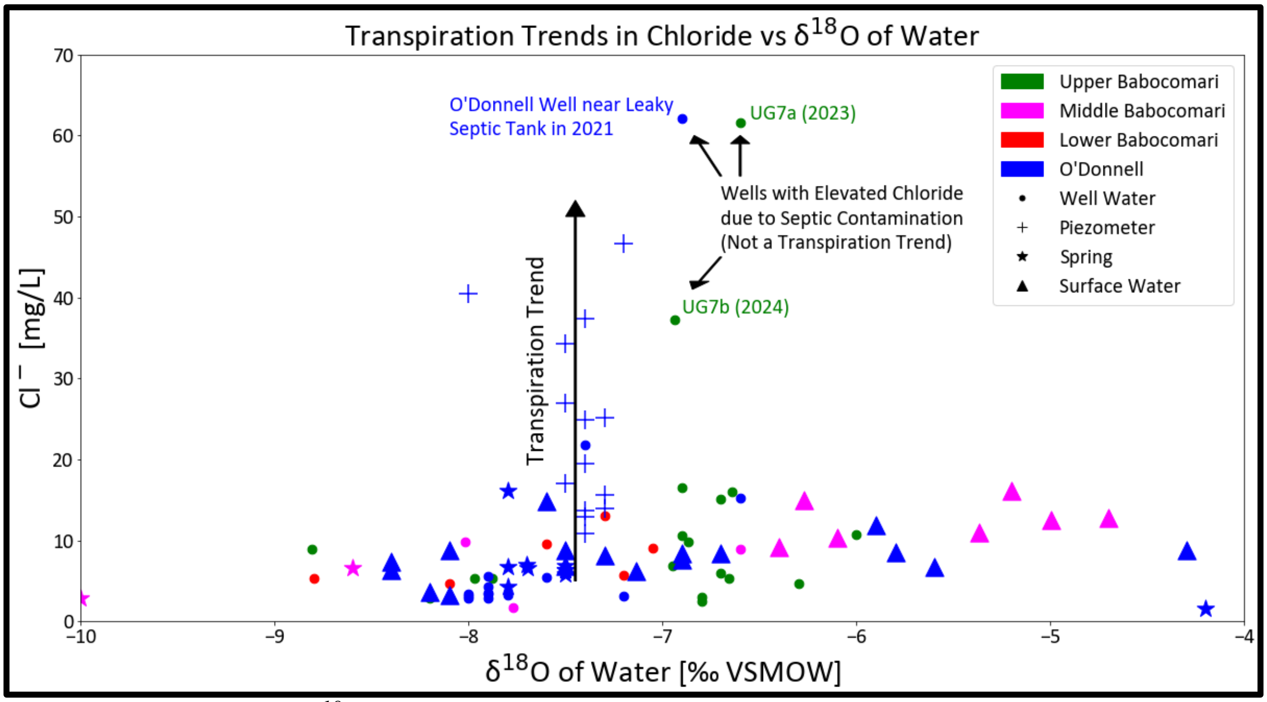

Figure 12: Chloride vs $\delta^{18}O$ of water reveals an increase in chloride concentration of O'Donnell Creek piezometer samples (blue crosses) with little change in $\delta^{18}O$ of water, which Stratman (2022) identified as a transpiration trend. No such trend is visible in the middle Babocomari Watershed samples (pink triangles), although a lack of shallow piezometer samples along the Babocomari Cienega and River makes it difficult to determine concretely the extent of transpiration in the middle Babocomari Watershed. To avoid misinterpretation, three wells on this graph have been labeled and identified as having elevated chloride due to septic contamination, not transpiration. This graph includes samples from this study, as well as from Schwartzmann (1990) and Stratman (2022).

Appendix B – Tables

Table 1. Sampling dates, times, and locations for each of the samples collected for this study. The sample ID indicates the sample's location (U = Upper Babocomari Watershed = U, M = Middle Babocomari Watershed, O = O'Donnell Creek subwatershed) and type (G = Groundwater, S = Surface water, P = Piezometer, R = Spring). Samples collected from the same sampling site but at a later date are indicated by an "a", "b", or "c" after their sample ID. A negative longitude means west of the Prime Meridian. Samples with no value are indicated by a lone hyphen ("-").

Sample ID	*Date [mm/dd/yy]*	*Collection Time*	*Latitude*	*Longitude*	*Elevation [ft]*
UG1a	2/18/23	-	31.6583	-110.5266	4750
UG1b	6/27/24	11:30 AM	31.6582	-110.52644	4847
UG2	2/18/23	-	31.5955	-110.5754	5070
UG3	7/6/23	9:30 AM	31.6823	-110.5635	4822
UG4	7/6/23	10:30 AM	31.6727	-110.5571	4797
UG5	7/6/23	11:00 AM	31.6595	-110.5428	4769
UG6a	7/6/23	11:45 AM	31.6604	-110.5826	4889
UG6b	6/27/24	12:00 PM	31.66035	-110.58256	4908
UG7a	7/6/23	12:30 PM	31.6082	-110.5890	5062
UG7b	6/27/24	1:00 PM	31.60824	-110.5890	5107
UG8	7/6/23	1:30 PM	31.6596	-110.6078	4931
UG9	8/5/23	10:00 AM	31.6392	-110.6101	4942
UG10a	8/5/23	11:00 AM	31.6413	-110.5267	4734
UG10b	6/27/24	2:30 PM	31.64109	-110.52654	4794
UG11	6/27/24	10:30 AM	31.6643	-110.5010	4601
UG12	6/27/24	1:30 PM	31.58869	-110.6070	5218
UG13	11/10/24	10:30 AM	31.7150	-110.5065	5046
MG1	8/5/23	1:00 PM	31.6438	-110.4151	4489
MG2a	8/5/23	2:00 PM	31.6318	-110.4500	4508
MG2b	11/10/24	1:30 PM	31.63186	-110.4500	4529
MG3	8/5/23	3:00 PM	31.6469	-110.4573	4676
MS1	8/5/23	5:30 PM	31.6304	-110.4628	4561
MS2	8/5/23	6:00 PM	31.6311	-110.4608	4541
MS3	4/20/24	10:30 AM	31.6349	-110.3780	4346
MS4a	4/20/24	11:30 AM	31.6319	-110.4015	4418
MS4b	11/10/24	2:30 PM	31.63191	-110.4022	4422
MS5	4/20/24	12:30 PM	31.6318	-110.4574	4613
MS6	4/20/24	1:30 PM	31.6337	-110.4594	4644
MS7a	4/20/24	2:30 PM	31.6309	-110.4522	4387
MS7b	11/10/24	12:30 PM	31.6312	-110.4519	4538
OP1a	2/18/23	-	31.5635	-110.5291	4950
OP1b	4/20/24	5:00 PM	31.5635	-110.5288	4945
OP2	2/18/23	-	31.5639	-110.5286	4940
OR1a	2/18/23	-	31.5623	-110.5294	4965
OR1b	4/20/24	5:30 PM	31.5624	-110.5293	4912
OR1c	11/10/24	4:45 PM	31.56228	-110.5293	4931
OS1a	2/18/23	-	31.5649	-110.5272	4930
OS1b	4/20/24	4:00 PM	31.5648	-110.5272	4885
OS2	11/10/24	5:00 PM	31.5633	-110.52811	4924

Table 2: Sample Stable Water Isotope Measurements. Samples with no value are indicated by a lone hyphen (“-“).

Sample ID	*$\delta^{18}O$ of H_2O [‰ VSMOW]*	*$\delta^{2}H$ of H_2O [‰ VSMOW]*
UG1a	-6.7	-50.3
UG1b	-6.6	-49.9
UG2	-6.9	-54.2
UG3	-6.3	-43.8
UG4	-6.8	-48.1
UG5	-6.8	-49.1
UG6a	-6.7	-49.6
UG6b	-6.7	-48.0
UG7a	-6.6	-54.4
UG7b	-6.9	-54.2
UG8	-6.0	-52.0
UG9	-8.8	-62.7
UG10a	-6.9	-52.7
UG10b	-6.9	-51.0
UG11	-8.2	-57.2
UG12	-7.9	-56.5
UG13	-8.0	-56.6
MG1	-7.8	-52.8
MG2a	-6.6	-49.1
MG2b	-	-
MG3	-8.0	-58.7
MS1	-6.3	-46.0
MS2	-5.0	-42.0
MS3	-6.1	-44.7
MS4a	-6.4	-45.1
MS4b	-5.4	-40.0
MS5	-4.7	-38.8
MS6	-3.8	-35.5
MS7a	-5.2	-40.6
MS7b	-2.1	-20.9
OP1a	-7.3	-53.8
OP1b	-7.4	-53.8
OP2	-7.3	-54.4
OR1a	-7.5	-54.2
OR1b	-7.5	-54.3
OR1c	-7.7	-54.9
OS1a	-6.9	-47.8
OS1b	-6.9	-48.9
OS2	-7.1	-50.5

Table 3: Sample Field Meter Measurements and calculated Total Dissolved Solids (TDS). Field meters were used to measure the pH, EC, temperature, and DO of all samples, while TDS was calculated by summing each sample's measured anion and cation concentrations in Tables 4a and 4b. Samples with no value are indicated by a lone hyphen ("-").

Sample ID	*pH*	*EC [µS/cm]*	*Temp [°C]*	*DO [%]*	*TDS [mg/L]*
UG1a	7.69	509.0	15.7	46.2	377.21
UG1b	7.64	518.0	24.7	68.7	389.00
UG2	7.55	432.0	17.9	62.4	342.79
UG3	7.20	423.3	24.4	81.9	295.84
UG4	7.41	431.2	21.1	75.2	296.29
UG5	7.38	404.7	21.6	84.1	287.45
UG6a	7.22	417.0	23.0	79.5	293.51
UG6b	7.55	364.0	23.0	77.9	292.90
UG7a	7.07	840.0	23.7	80.1	522.55
UG7b	7.24	616.5	21.7	81.3	466.35
UG8	7.32	349.5	23.4	99.5	273.31
UG9	7.40	312.3	21.4	83.6	253.70
UG10a	7.13	508.6	19.6	68.1	365.77
UG10b	7.19	471.7	21.9	80.5	366.27
UG11	8.67	363.9	25.3	60.4	310.92
UG12	6.98	554.2	27.4	81.2	459.00
UG13	7.38	386.5	20.4	77.3	293.46
MG1	7.36	670.9	24.2	77.3	445.15
MG2a	7.00	687.4	18.2	35.5	488.81
MG2b	7.06	552.8	17.2	39.6	-
MG3	7.22	576.2	22.4	58.2	401.87
MS1	6.61	1100	25.0	1.7	714.24
MS2	6.96	759.3	29.8	12.3	598.01
MS3	7.87	726.1	15.9	68.7	573.39
MS4a	7.20	717.6	15.9	74.5	577.91
MS4b	7.67	663.0	8.0	37.0	540.82
MS5	7.08	926.7	26.9	2.0	779.95
MS6	7.42	791.3	18.2	24.0	637.77
MS7a	7.95	776.6	19.7	110.0	614.31
MS7b	7.38	426.6	14.3	85.3	330.34
OP1a	7.20	850.0	7.4	5.7	709.36
OP1b	7.20	940.5	13.9	26.6	731.72
OP2	7.07	1003	-	6.2	856.73
OR1a	6.76	590.0	19.4	26.0	480.06
OR1b	7.28	653.6	19.2	38.7	499.88
OR1c	6.96	554.3	19.6	25.8	-
OS1a	7.67	544.0	6.0	65.8	442.99
OS1b	7.72	726.6	14.8	60.0	577.86
OS2	7.33	583.9	8.0	33.3	513.85

Table 4a: Sample Major Ion Chemistry (Anions). Bicarbonate (HCO_3^-) is considered equivalent to alkalinity in natural waters with near-neutral pHs. "BDL" = "Below Detection Limit" (less than 5.00µmol/L for anions). Samples with no value are indicated by a lone hyphen ("-").

Sample ID	*HCO_3^- [mg/L]*	*F^- [mg/L]*	*Cl^- [mg/L]*	*NO_2^- [mg/L]*	*Br^- [mg/L]*	*NO_3^- [mg/L]*	*PO_4^{3-} [mg/L]*	*SO_4^{2-} [mg/L]*
UG1a	191.52	0.61	15.10	BDL	0.23	17.89	BDL	55.48
UG1b	192.92	0.54	15.99	BDL	0.24	13.90	BDL	54.02
UG2	234.71	0.28	16.53	BDL	0.21	6.62	BDL	5.35
UG3	219.82	0.37	4.71	BDL	0.12	4.03	BDL	0.73
UG4	219.03	0.29	2.48	BDL	0.11	3.13	BDL	0.81
UG5	208.53	0.28	2.96	BDL	0.12	3.14	BDL	1.01
UG6a	213.63	0.40	5.94	BDL	0.12	3.45	BDL	1.72
UG6b	213.87	0.35	5.26	BDL	0.22	2.93	BDL	1.55
UG7a	261.29	0.50	61.64	BDL	0.25	52.37	BDL	21.25
UG7b	255.98	0.25	37.31	BDL	0.31	34.21	BDL	14.40
UG8	192.09	0.56	10.74	BDL	0.14	5.01	BDL	1.19
UG9	166.39	0.14	8.94	BDL	0.15	8.38	BDL	7.85
UG10a	257.75	0.17	10.59	BDL	0.17	2.75	BDL	6.24
UG10b	258.18	0.15	9.86	BDL	0.20	2.18	BDL	5.94
UG11	206.54	0.23	2.92	BDL	0.18	1.61	BDL	10.23
UG12	341.53	0.19	5.34	BDL	0.22	2.31	BDL	2.92
UG13	210.10	0.60	5.32	BDL	0.23	2.69	BDL	5.06
MG1	225.44	0.50	1.75	BDL	BDL	2.56	BDL	104.80
MG2a	332.13	0.24	8.86	BDL	0.22	3.46	BDL	27.81
MG2b	306.89	-	-	-	-	-	-	-
MG3	275.44	0.30	9.81	BDL	0.18	5.84	BDL	15.80
MS1	524.56	0.24	14.94	BDL	0.28	0.29	BDL	3.72
MS2	424.14	0.30	12.51	BDL	0.29	0.11	BDL	18.71
MS3	392.60	0.28	10.39	BDL	0.54	BDL	BDL	25.39
MS4a	397.71	0.27	9.19	BDL	0.48	BDL	BDL	24.97
MS4b	361.87	0.25	10.93	BDL	0.26	BDL	BDL	31.14
MS5	525.81	0.43	12.73	BDL	0.53	BDL	BDL	47.45
MS6	443.35	0.33	15.22	BDL	0.50	BDL	BDL	11.97
MS7a	388.44	0.35	16.16	BDL	0.56	BDL	BDL	49.50
MS7b	204.49	0.19	5.18	BDL	0.21	BDL	BDL	32.62
OP1a	533.29	0.25	15.59	BDL	0.26	BDL	BDL	12.94
OP1b	508.75	0.27	24.92	BDL	0.52	BDL	BDL	20.32
OP2	635.19	0.38	25.13	BDL	0.35	0.07	BDL	14.32
OR1a	366.71	0.19	6.91	BDL	0.20	0.88	BDL	6.73
OR1b	372.11	0.24	6.30	BDL	0.41	0.64	BDL	6.17
OR1c	369.95	0.17	6.56	BDL	0.13	0.68	BDL	6.05
OS1a	333.76	0.22	8.43	BDL	0.22	BDL	BDL	8.95
OS1b	388.47	0.32	7.70	BDL	0.45	BDL	BDL	43.77
OS2	372.72	0.27	6.17	BDL	0.19	BDL	BDL	12.03

Table 4b: Sample Major Ion Chemistry (Cations). Samples with no value are indicated by a lone hyphen ("-").

Sample ID	*Na^+ [mg/L]*	*Mg^{2+} [mg/L]*	*K^+ [mg/L]*	*Ca^{2+} [mg/L]*
UG1a	73.98	2.57	1.37	18.44
UG1b	77.18	2.77	1.34	30.09
UG2	34.18	19.35	1.33	24.23
UG3	17.23	11.04	4.39	33.40
UG4	29.02	11.94	3.05	26.43
UG5	38.58	4.22	1.97	26.66
UG6a	23.44	22.71	1.99	20.11
UG6b	19.64	19.18	1.64	28.28
UG7a	39.95	14.62	1.04	69.65
UG7b	38.16	8.99	0.90	75.83
UG8	18.38	9.20	3.96	32.05
UG9	7.32	3.41	1.16	49.94
UG10a	23.73	12.44	2.10	49.84
UG10b	24.29	12.72	1.98	50.77
UG11	82.67	0.20	0.71	5.64
UG12	7.19	18.24	0.89	80.16
UG13	6.80	15.03	2.26	45.38
MG1	14.71	22.58	2.94	69.87
MG2a	17.51	13.25	2.71	82.62
MG2b	-	-	-	-
MG3	7.24	12.30	2.21	72.74
MS1	22.60	17.97	11.74	117.89
MS2	20.94	15.46	7.10	98.43
MS3	21.50	16.64	2.79	103.27
MS4a	19.49	15.77	1.86	108.17
MS4b	20.40	16.20	2.67	97.09
MS5	24.79	20.08	1.70	146.42
MS6	30.17	19.47	10.71	106.06
MS7a	30.02	20.56	2.98	105.73
MS7b	10.88	9.07	6.59	61.12
OP1a	37.55	30.40	0.90	78.19
OP1b	39.54	32.43	0.68	104.29
OP2	63.00	38.93	2.68	76.69
OR1a	15.28	16.69	1.47	65.00
OR1b	14.72	18.01	1.40	79.87
OR1c	13.89	17.24	1.25	90.36
OS1a	10.53	13.73	2.40	64.73
OS1b	10.71	15.75	2.18	108.52
OS2	8.28	13.34	1.78	99.07

Table 5: Sample δ^{13}C-DIC, Tritium, and Radiocarbon measurements. Surface water samples were not analyzed for radiocarbon since it was assumed they were already in equilibrium with atmospheric carbon. For tritium, "BDL" = "Below Detection Limit" (<0.5 to <0.6 TU), meaning the sample did not have a component of modern recharge (i.e., no recharge after the 1950s). Samples with no value are indicated by a lone hyphen ("-").

Sample ID	*δ^{13}C-DIC [‰ VPDB]*	*Tritium [TU]*	*Radiocarbon [pMC]*	*Radiocarbon Uncorrected Age [yrs]*	*Radiocarbon Corrected Age [yrs]*
UG1a	-3.4	BDL	49.15	5,710	Submodern (<500 Years)
UG1b	-	-	-	-	-
UG2	-1.4	BDL	16.92	14,250	Submodern (<500 Years)
UG3	-4.3	BDL	42.48	6,880	Submodern (<500 Years)
UG4	-3.7	BDL	38.86	7,590	Submodern (<500 Years)
UG5	-2.8	BDL	52.60	5,160	Submodern (<500 Years)
UG6a	-4.7	BDL	-	-	-
UG6b	-	-	-	-	-
UG7a	-6.7	1.3	93.26	560	Submodern (<500 Years)
UG7b	-	-	-	-	-
UG8	-2.4	1.1	47.78	5,930	Submodern (<500 Years)
UG9	-4.8	1.3	86.78	1,140	Submodern (<500 Years)
UG10a	-6.1	BDL	-	-	-
UG10b	-	-	-	-	-
UG11	-10.1	BDL	55.97	4,660	Submodern (<500 Years)
UG12	-5.5	0.5	-	-	-
UG13	-3.5	BDL	-	-	-
MG1	-6.9	BDL	-	-	-
MG2a	-7.5	2.8	-	-	-
MG2b	-	-	-	-	-
MG3	-6.7	0.6	70.97	2,750	Submodern (<500 Years)
MS1	-5.4	3.3	-	-	-
MS2	-2.6	3.0	-	-	-
MS3	-7.8	3.2	-	-	-
MS4a	-7.9	3.2	-	-	-
MS4b	-7.6	3.3	-	-	-
MS5	-9.5	3.1	-	-	-
MS6	-5.4	3.2	-	-	-
MS7a	-6.8	0.6	-	-	-
MS7b	-5.4	7.8	-	-	-
OP1a	-10.5	-	-	-	-
OP1b	-10.7	3.0	-	-	-
OP2	-11.2	-	-	-	-
OR1a	-6.9	-	-	-	-
OR1b	-8.5	BDL	-	-	-
OR1c	-9.8	BDL	-	-	-
OS1a	-8.6	1.4	-	-	-
OS1b	-10.7	2.1	-	-	-
OS2	-11.6	1.3	-	-	-

Table 6: Nitrate Isotope Measurements. Nitrate isotopes were only measured in two samples with elevated nitrate concentrations.

Sample ID	*$\delta^{15}N$ of NO_3^- [‰ AIR]*	*$\delta^{18}O$ of NO_3^- [‰ VSMOW]*
UG1b	12.3	9.8
UG7b	8.3	1.1

References

Arizona Department of Water Resources. (2020). *Water Your Facts*. Arizona Water Facts. https://www.arizonawaterfacts.com/water-your-facts

Arizona Department of Water Resources. (2023). *2023 Supply and Demand Assessment—Willcox Basin.* [Report]. https://www.azwater.gov/sites/default/files/2023-12/2023_WillcoxBasin.pdf

Arizona Department of Water Resources. (2024). *Groundwater Conditions of the Willcox Basin*. [Memorandum]. https://www.azwater.gov/sites/default/files/2024-10/2024_10-21_ADWR%20Memorandum%20Willcox%20Basin%20Groundwater%20Conditions.pdf.

Babacomari Ranch. (n.d.). Retrieved September 28, 2023, from www.babacomariranch.com.

Baillie, M. N. (2005). *Quantifying baseflow inputs to the San Pedro River: a geochemical approach,* (Master's thesis). Retrieved from UA Campus Repository. (http://hdl.handle.net/10150/192125). Tucson, AZ: University of Arizona.

Craig, H. (1961). Isotopic Variations in Meteoric Waters. *Science, 133,* 1702-1703. https://doi.org/10.1126/science.133.3465.1702

Davison, L. (2023). County Plans to Develop Winery District Master Plan. *Patagonia Regional Times. https://patagoniaregionaltimes.org/county-plans-to-develop-winery-district-master-plan/*

Dubrovsky, N.M., Burow, K.R., Clark, G.M., Gronberg, J.M., Hamilton P.A., Hitt, K.J., et al. (2010). The quality of our Nation's waters—Nutrients in the Nation's streams and groundwater, 1992-2004: *U.S. Geological Survey Circular 1350.* https://pubs.usgs.gov/circ/1350/pdf/circ1350.pdf

Eastoe, C. J., & Dettman, D. L. (2016). Isotope amount effects in hydrologic and climate reconstructions of monsoon climates: Implications of some long-term data sets for precipitation. *Chemical Geology, 430,* 78-89. https://doi.org/10.1016/j.chemgeo.2016.03.022

Eastoe, C. J., & Towne, D. (2018). Regional zonation of groundwater recharge mechanisms in alluvial basins of Arizona: Interpretation of isotope mapping. *Journal of Geochemical Exploration, 194*, 134-145. https://doi.org/10.1016/j.gexplo.2018.07.013.

Eastoe, C. J., & Wright, W. E. (2019). Hydrology of Mountain Blocks in Arizona and New Mexico as Revealed by Isotopes in Groundwater and Precipitation. *Geosciences, 9*(11), 461. https://doi.org/10.3390/geosciences9110461

Environmental Protection Agency. (2024a). *Climate Change Indicators: Heavy Precipitation.* United States Environmental Protection Agency. https://www.epa.gov/climate-indicators/climate-change-indicators-heavy-precipitation

Environmental Protection Agency. (2024b). *National Drinking Water Regulations*. United States Environmental Protection Agency. https://www.epa.gov/ground-water-and-drinking-water/national-primary-drinking-water-regulations

Gibrilla, A., Fianko, J. R., Ganyaglo, S., Adomako, D., Anornu, G., & Zakaria, N. (2020). Nitrate contamination and source apportionment in surface and groundwater in Ghana using dual isotopes (15N and 18O-NO3) and a Bayesian isotope mixing model. *Journal of Contaminant Hydrology, 233,* 103658. https://doi.org/10.1016/j.jconhyd.2020.103658.

Han, L.-F., & Plummer, L.N. (2013). Revision of Fontes & Garnier's model for the initial ^{14}C content of dissolved inorganic carbon used in groundwater dating. *Chemical Geology*, 351, 105-114. https://doi.org/10.1016/j.chemgeo.2013.05.011.

Hendrickson, D. A., & Minckley, W. L. (1985). Ciénegas-Vanishing climax communities of the American Southwest. *Desert Plants, 6(3),* 131-175. http://dx.doi.org/10.26153/tsw/9234.

Hopkins, C. B., McIntosh, J. C., Eastoe, C., Dickinson, J. E., Meixner, T. (2014). Evaluation of the importance of clay confining units on groundwater flow in alluvial basins using solute and isotope tracers: the case of Middle San Pedro Basin in southeastern Arizona (USA). *Hydrogeology Journal, 22,* 829–849. https://doi.org/10.1007/s10040-013-1090-0.

Ingraham, N. L. (1998). Isotopic Variations in Precipitation. In C. Kendall, J. J. McDonnell (Eds.), *Isotope Tracers in Catchment Hydrology* (pp. 87-118). Amsterdam: Elsevier Science B.V. https://doi.org/10.1016/B978-0-444-81546-0.50010-0

Jasechko, S. (2019). Global Isotope Hydrogeology—Review. *Reviews of Geophysics, 57*(3), 835-965. https://doi.org/10.1029/2018RG000627

Jolliffe, I. T. (2002). *Principal component analysis* (2nd ed.). New York City, NY: Springer.

Kendall, C. (1998). Tracing Nitrogen Sources and Cycling in Catchments. In C. Kendall, J. J. McDonnell (Eds.), *Isotope Tracers in Catchment Hydrology* (pp. 519-576). Amsterdam: Elsevier Science B.V. https://doi.org/10.1016/B978-0-444-81546-0.50023-9.

Kirk, A. G. (2020). *A Hydrochemical Modeling Study to Evaluate Potential Regional and Local Flowpaths to Surface Water Base Flow in Lower Cienega Creek and Davidson Canyon, Southeastern Arizona*, (Master's thesis). Retrieved from UA Campus Repository. (http://hdl.handle.net/10150/645777). Tucson, AZ: University of Arizona.

Knight, E. L. (1996). *A water budget and land management recommendations for Upper Cienega Creek Basin*. (Master's thesis). Retrieved from UA Campus Repository. (http://hdl.handle.net/10150/191300). Tucson, AZ: University of Arizona.

Minckley, T. A., Turner, D. S., & Weinstein, S. R. (2013). The relevance of wetland conservation in arid regions: A re-examination of vanishing communities in the American Southwest. *Journal of Arid Environments, 88,* 213-221. https://doi.org/10.1016/j.jaridenv.2012.09.001.

Myskow, W. (2023). Rural Arizona Has Gone Decades Without Groundwater Regulations. That Could Soon Change. *Inside Climate News*. *https://insideclimatenews.org/news/19122023/rural-arizona-decades-without-groundwater-regulations/*

Naeser, R., & St. John, A. (1998). *Water use and the future of the Sonoita Valley*, 186-200. University of Arizona Press: Tucson, AZ, USA. https://www.fs.usda.gov/rm/pubs/rmrs_p003/rmrs_p003_186_200.pdf

Montgomery & Associates and Natural Channel Design Engineering Inc. (2025). *Babocomari Watershed Assessment*. Consultant's report to The Nature Conservancy, Tucson, Arizona.

Norman, L., Callegary, J., Lacher, L., Wilson, N., Fandel, C., Forbes, B., & Swetnam, T. (2019). Modeling Riparian Restoration Impacts on the Hydrologic Cycle at the Babacomari Ranch, SE Arizona, USA. *Water*, *11*(2), 381. MDPI AG. http://dx.doi.org/10.3390/w11020381

Peterson, J. A., Berquist, J. R., Reynolds, S. J., & Page-Nedell, S. S. (2001). *Geologic map of the Tucson and Nogales quadrangles (Arizona, scale 1:250,000): a digital database* (Open-File Report OF-2001-275, scale 1:250,000). Retrieved from National Geologic Map Database. (https://ngmdb.usgs.gov/Prodesc/proddesc_54505.htm). Arizona: U.S. Geological Survey.

Robinett, D. & Kennedy, L. (2013). *Babocomari river riparian protection project.* Paper presented at Merging science and management in a rapidly changing world: Biodiversity and management of the Madrean Archipelago III and 7th Conference on Research and Resource Management in the Southwestern Deserts, USDA Forest Service, Rocky Mountain Research Station, Tucson, AZ. https://www.fs.usda.gov/rm/pubs/rmrs_p067/rmrs_p067_490_492.pdf.

Santa Cruz County Government. (2024). *Santa Cruz County Seeking Community Members to Join Southern Arizona Culinary Tourism Steering Committee* [Press release]. https://www.santacruzcountyaz.gov/DocumentCenter/View/18429/PRESS-RELEASE_-Jan-2024-Santa-Cruz-County-Cuisine-Tourism-Initiative?bidId=

Schwartzman, P. N. (1990). *A hydrogeologic resource assessment of the lower Babocomari Watershed, Arizona,* (Master's thesis). Retrieved from UA Campus Repository. (http://hdl.handle.net/10150/192030). Tucson, AZ: University of Arizona.

Stratman, A. L. (2022). *Origins and residence times of water supporting O'Donnell Creek Cienega in southeastern Arizona,* (Master's thesis). Retrieved from UA Campus Repository. (http://hdl.handle.net/10150/665022). Tucson, AZ: University of Arizona.

Tritz, C. (2021). *Tracing and Quantifying Mountain Block Recharge in the Northern Santa Rita Mountains Via End-Member Mixing and Chloride Mass Balance Analyses*, (Master's thesis). Retrieved from UA Campus Repository. (http://hdl.handle.net/10150/660220). Tucson, AZ: University of Arizona.

Tucci, R. (2018). *Using isotopes and solute tracers to infer groundwater recharge and flow in the Cienega Creek Watershed, SE Arizona,* (Master's thesis.) Retrieved from UA Campus Repository. (http://hdl.handle.net/10150/628442). Tucson, AZ: University of Arizona.

University of Arizona Environmental Isotope Laboratory. (2022). *Tritium and stable isotope data for seasonal aggregate precipitation samples, Tucson and Payson, AZ.* (Dataset). Retrieved from Environmental Isotope Laboratory Data Repository. (https://www.geo.arizona.edu/sites/www.geo.arizona.edu/files/pictures/Tritium_Tucson_Payson_AZ_Nov22.xlsx). Tucson, AZ: University of Arizona.

USDOI Bureau of Land Management (2022). *Babocomari land health evaluation.* https://eplanning.blm.gov/public_projects/2013674/200485202/20058771/250064953/FINAL%20Babocomari%20LHE_April%202022.pdf.

Vendituoli, M. (2024). County Pivots Initiative After Community Outcry. *Patagonia Regional Times*. https://patagoniaregionaltimes.org/county-pivots-initiative-after-community-outcry/

Vicenti, N. C. (2018). *Natural Tracer Study to Constrain Transit Times and Flowpaths of Groundwater from Davidson Canyon to Lower Cienega Creek,* (Master's thesis). Retrieved from UA Campus Repository. (http://hdl.handle.net/10150/631406). Tucson, AZ: University of Arizona.

Vukomanovic, J., Vogler, J. B., & Petrasova, A. (2019). Modeling the connection between viewscapes and home locations in a rapidly exurbanizing region. *Computers, Environment and Urban Systems*, *78(2)*, 101388. https://doi.org/10.1016/j.compenvurbsys.2019.101388

Wahi, A. K. (2005) *Quantifying mountain system recharge in the upper San Pedro basin, Arizona, using geochemical tracers,* (Master's thesis). Retrieved from UA Campus Repository. (http://hdl.handle.net/10150/626932). Tucson, AZ: University of Arizona.